THE WEST ANTARCTIC ICE SHEET: BEHAVIOR AND ENVIRONMENT
ANTARCTIC RESEARCH SERIES, VOLUME 77, PAGES 157-199

BASAL ZONE OF THE WEST ANTARCTIC ICE STREAMS AND ITS ROLE IN LUBRICATION OF THEIR RAPID MOTION

Barclay Kamb

Division of Geological and Planetary Sciences, California Institute of Technology, Pasadena, California

Basal processes and conditions at the bottom of ice streams B, C, and D and under adjacent parts of interstream ridges B1-B2 and C-D have been studied via boreholes drilled to the base of the ice by the hot-water jet drilling method. The objective is to reveal on an observational basis the mechanism of rapid ice-streaming motion as a guide to theoretical models of the ice-stream phenomenon in the West Antarctic Ice Sheet. Whereas the ice sheet outside the ice streams is frozen to its bed, the base of the ice streams is at the melting point and water is available there at a pressure close to the ice overburden pressure, so that the effective pressure is near zero. These conditions are favorable for both basal sliding and deformation of soft basal sediments as mechanisms for lubrication of rapid ice-stream motion. Sediments consisting of unfrozen glacial till are present at the base of the ice streams in a layer $\lesssim$10 m thick. Frozen basal till is present under interstream ridges with a prior history of streaming motion. The till's lithological characteristics reflect derivation from Tertiary glacimarine sediments of the Ross Sea sequence, which are thought to underlie the till layer. The water content of the unfrozen till is high, corresponding to water-saturated bulk porosities ranging from 26% to 58%. The high porosity is compatible with till deformation under low effective pressure. Except for extensive breakage of diatom tests and mixing of diatom ages, and except possibly for the occurrence of prominent "skelsepic plasmic" fabrics, the till does not show unambiguous internal evidence of deformation. This is probably because a "cushioning" action of the clay-rich matrix under low effective pressure shields the rock particles from abrasion and comminution. Till deformation is however indicated by measurements of basal sliding made with the tethered stake instrument. They show that in Ice Stream D about 80% of the motion was by till deformation whereas in Ice Stream B only about 25% was. The large, as-yet unexplained difference between the two ice streams in the relative contributions of till deformation and basal sliding to their streaming motions constitutes a challenge to understanding the ice stream mechanism, as does the time variation in these contributions. Mechanical tests of the till in the field and in the laboratory (direct shear, ring-shear, and triaxial tests on till cores, plus in-situ tests with a torvane instrument) were used to investigate the till rheology, which probably plays an important role in the ice stream mechanism. The need is to distinguish among quasiviscous rheology, treiboplastic (Coulomb-plastic) rheology, and possibly a hybrid of the two. The till has a well-defined yield stress that depends linearly on the effective pressure and only slightly on the shear strain rate. These are characteristics of treiboplastic rheology. The internal friction is 0.45±0.02 and the apparent cohesion is small (~ 1 kPa). The strength depends inversely on till porosity and tends to increase at deeper levels in the till. The slight strain-rate dependence amounts on average to a 5% increase in strength per decade increase in strain rate. This type of dependence can be represented empirically as a power-type flow law

with a very large value of the exponent, $n \sim 40$, very much larger than the $1 \leq n \leq 5$ typical of viscous or quasiviscous rheologies. The strain-rate dependence can be explained as the result of measurable pore-pressure changes induced by changes in strain rate. Observations in Ice Stream D establish the existence of a basal water conduit system that in its natural state, unmodified by effects of borehole drilling, is capable of delivering a substantial quantity of water at a pressure approximately equal to the ice overburden pressure. Damped oscillations of the borehole water level are compatible with a "gap conduit" model in which the conduits form a 2.5-mm water-filled gap between the base of the ice and the top of the till. A diagnostic parameter for the gap width is the time that it takes for the borehole water level to drop from an initial shallow depth to a final depth near 105 m when a borehole being drilled breaks through into the basal water system. For Ice Streams B and D this drop time is mostly in the range 1-3 minutes, whereas the boreholes in Ice Stream C tend to have drop times distinctly longer, in the range 5-30 minutes, suggesting a tendency for thinner gap-conduits in its basal water system. An extreme case is a borehole drilled in the fossil marginal shear zone, in which the drop time was 5 hours. Problems in interpretation of the basal water system and ice streaming mechanism in terms of the observed basal water pressures and calculated ice overburden pressures are discussed. A large difference in some well defined flow-controlling variable is expected on comparing Ice Streams B and D with Ice Stream C, whose rapid streaming motion came nearly
to a stop about 150 years ago. But despite the great difference in flow velocity (B and D ca. 1 m d^{-1}, C ca. 0.04 m d^{-1}), these three ice streams appear quite similar in terms of the physical conditions and structures (till layer, water conduit system) found by borehole observation of their basal zones. The a-priori most likely controlling variable, the basal effective pressure, has average values (0.2×10^5 Pa for C, 0.6×10^5 Pa for B, 0.4×10^5 Pa for D) that differ in the wrong way to explain the slowing of Ice Stream C. However, there are a few subtle differences that may point indirectly to what has caused the slowdown: (1) indications of freeze-on at the base of Ice Stream C; (2) thinner gap-conduits in the basal water system of Ice Stream C; (3) in-situ shear strength of basal till under Ice Stream C (5 kPa) is higher than that under Ice Streams B and D (2 kPa, 1 kPa). According to a new theory of ice-stream soft-bed mechanics by S. Tulaczyk, the increased till strength under Ice Stream C is about great enough to switch the ice stream from a stable state of high velocity to an unstable state of lower velocity that decays with time and leads to ice-stream shut down. It appears that the streaming flow of Ice Stream C has not completely shut down in the area studied, which to some extent explains the similarity in physical conditions with those of Ice Streams B and D.

1. INTRODUCTION

Ever since the discovery of the great ice streams in the West Antarctic Ice Sheet (WAIS), with flow speeds ~10-100 times faster than the non-streaming adjacent parts of the ice sheet [*Bentley*, 1987; *Bindschadler and Scambos*, 1991; *Whillans and van der Veen*, 1993; *Bindschadler et al.*, 1996; *Joughin et al.*, 1999; *Doake et al.*, 1987; *Smith*, 1997], there has been a pressing need to understand the ice stream flow mechanism so that the role of the ice streams in the configuration and stability of WAIS could be rationally assessed. Such an assessment is needed as part of the overall effort to predict the future behavior of WAIS in relation to possible climate change and possible change of world-wide sea level [*Mercer*, 1978; *Alley and Whillans*, 1991; *Alley and MacAyeal*, 1993; *Oppenheimer*, 1998; *Bindschadler et al.*, 1998; *Bentley*, 1998]. The flow mechanism is recognized also as a fundamental problem in glaciology, possibly involving phenomena quite different from those in normal glacier flow. Three candidate mechanisms have been proposed for the rapid ice streaming flow: (1) enhanced basal- and marginal-ice shear deformation due to stress-induced recrystallization [*Hughes*, 1977]; (2) basal sliding due to basal melting [*Rose et al.*, 1979]; and (3) lubrication of the bed by soft basal sediment [*Alley et al.*, 1986]. (1) and (2) are conventional mechanisms, already much studied in glaciology, whereas (3) was put forward as a new paradigm

of glacier mechanics by *Boulton* [1986] and is only now getting full attention as a glacier flow mechanism. It was proposed as the mechanism for ice stream flow by *Blankenship et al.* [1986] on the basis of reflection seismic data from Ice Stream B, and it has been extensively discussed in a series of papers by these authors [*Blankenship et al.*, 1987; *Rooney et al.*, 1987; *Alley et al.*, 1987a, 1987b, 1989, 1994; *Alley*, 1989a, 1989b, 1993, 1994; *Cuffey and Alley*, 1996]. These papers paint an attractive, largely theoretical picture of mechanism (3), which has led to a rather general acceptance of (3) over (1) and (2) by the WAIS research community.

The present paper summarizes the results of a complementary, largely observational approach that endeavors to make direct in-situ observations of the ice stream mechanism and the physical conditions and processes that make it function and control it. The objective is to distinguish among (1), (2), and (3) on a comprehensive observational basis. Since the proposed mechanisms all involve processes at or near the base of the ice, to make direct in-situ observations of them requires drilling boreholes to the bed and deploying instruments there. Although this may appear to be a straightforward approach, in practice various complications and apparent contradictions in data interpretation have arisen, such that, as will be evident below, an unambiguous observational concept of the ice stream mechanism is yet to be achieved. For this reason the paper should be viewed as a progress report on this effort rather than a final statement on the mechanics of ice stream motion. Some of the results have been reported by *Engelhardt et al.* [1990], *Kamb* [1991], *Scherer* [1991, 1994], *Jackson and Kamb* [1997], *Engelhardt and Kamb* [1993, 1997, 1998], *Jackson* [1998] *Scherer et al.* [1998], *Tulaczyk* [1999], Jackson [1999], *Tulaczyk et al.* [1998, 2000a, 2000b, 2000c], and Engelhardt et al [2000]. The reference *Engelhardt and Kamb* [1997] is used so frequently that it is here abbreviated "E & K".

2. OBSERVATIONAL METHODS AND STUDY SITES

In our program, boreholes to the base of the ice, typically 1000-1200 m deep, are drilled by the hot-water jet drilling method with thermal power of approximately 480 kW, producing water-filled holes of nominal 10 cm diameter in approximately 15 hours of drilling. Completed holes are normally reamed for safety's sake to a minimum diameter of 10 cm by a hot-water reaming tool, requiring about 12 hours of reaming time. Instruments of diameter 5 cm are deployed in such holes for periods of up to about 4 hours without getting caught by freeze-in of the borehole wall under the ambient ice temperature of about –20 C. For more extended access the instruments are either allowed to freeze in or are removed and the hole rereamed to diameter 10 cm. The alternative of stabilizing the hole against refreezing by introducing antifreeze (ethanol) has been tried but was not generally successful. The individual borehole instruments are indicated in the following survey of the types of observations made and the results obtained.

Borehole observations have been made at five nearby "study sites" on Ice Stream B2 (hereafter called simply B), at six nearby sites on Ice Stream C, and at one site on Ice Stream D; also at three nearby sites on interstream Ridge B1-B2 (the Unicorn) and at two nearby sites on Ridge C-D (Siple Dome). The location of these sites is shown in Figure 1, in which the nearby sites are plotted together as single locations. "Nearby" in this context means within about 10 km of one another. On Ice Stream C, one of the sites is about 25 km distant from the other five and has other special characteristics discussed later. Four of the sites on Ice Stream B were close to the surface location of Camp Up B in different years, but because of the 0.44 km a^{-1} ice stream motion these sites sample basal conditions at locations 0.4-0.9 km apart; the fifth site was located about 10 km upstream from Up B, close to Camp New B. At each of these sites, usually several (1 to 13) individual boreholes were drilled, the number depending on the number and types of borehole observations wanted and on the successfulness of the holes in attaining specified objectives. Figure 2 shows in map view the borehole pattern at the study sites on Ice Stream C, drilled in the 1996-97 season; the pattern of boreholes in Ice Stream B (at Up B and New B) is given in E & K, Figure 2. The individual boreholes are identified by a number of the form "96-1", where "96" is the field season when the hole was drilled (1996-97) and "1" is the number of the borehole counted sequentially in time in that field season. The boreholes are listed in Table 1. The appearance of a typical drill site during drilling is shown in Figure 3.

The rationale for choosing the foregoing study sites was as follows. Initially the choice was Ice Stream B near Up B because this is where the seismic work that indicated a soft basal sediment layer had been done. The 10-km move to Up B '95 was made in order to sample basal conditions in an area where, according to the seismic work, the basal sediment layer was thin or absent and therefore a "sticky spot" with slow ice-stream motion might be expected. Ice Stream D was chosen to provide observations in a separate rapidly moving ice stream, for comparison with Ice Stream B. Ice Stream C was chosen to provide comparison with an ice stream whose rapid motion slowed down greatly about 150 years ago [*Shabtaie and Bentley*, 1987]. The

sites on interstream ridges (Unicorn and Siple Dome) provide information on basal conditions in the non-streaming ice sheet away from the ice streams, although the location of these particular sites was chosen primarily for other reasons.

3. PHYSICAL CONDITIONS IN THE BASAL ZONE

3.1 Temperature

Basal and englacial temperatures were measured in selected boreholes, normally one per study site, with thermistors enclosed in pressure-tight cases and calibrated to an accuracy of ±0.02 C. The thermistors were introduced into the measurement hole at predetermined depths via cables, the hole was allowed to freeze in, and the temperature of each thermistor was followed with time as it asymptotically approached a final temperature equal to the ambient temperature at the thermistor's depth. Details of the technique are given by *Engelhardt and Kamb* [1993]. Typical results are shown in Figure 4, which compares the vertical profile of temperature in an ice stream (at Up B) and in an interstream ridge (B1-B2, known as the Unicorn). The main difference is that the measured basal temperature in the ice stream (–0.82 C) is close to the pressure melting point (calculated as –0.71 C for ice 1057 m thick), whereas outside the ice stream the basal temperature is below the pressure melting point by amounts ranging from 0.6 to 2.7 degrees C at different study sites.

An independent indication of the distinction in basal temperature between the ice streams and the non-streaming ice sheet is that free water in a conduit system is almost always encountered at the base of the ice streams but is not encountered under the inter-stream ridges. This is further discussed in Section 7.

The base of ice Stream C presents a special situation, the basal temperature (measured in boreholes 96-2 and 96-12) lying 0.35 C below the calculated melting point. While the 0.1-degree discrepancy between measured basal temperature and calculated basal melting point for Ice Stream B can possibly be ascribed to measurement and/or calculation error, this does not seem possible for the 0.35 degree discrepancy for Ice Stream C in relation to the thermistor calibration accuracy of ± 0.02 C. This situation is discussed further in Sections 4.6 and 8.3.

The simple, straightforward conclusion is that ice streams form only where basal ice reaches the melting point. This conclusion was drawn by *Bentley et al.* [1998] from radar reflection data and was originally advocated on a theoretical basis by *Rose* [1979]. In Section 4.6 it will be shown that the basal temperature situation is somewhat more complicated but that the simple conclusion still holds, although with possible question as to its applicability to Ice Stream C.

3.2 Pressure

Three basal pressure quantities are important in ice stream mechanics: the ice overburden pressure (ice pressure) at the bed, the pressure of water having access to the bed, and the pore water pressure in basal sediments.

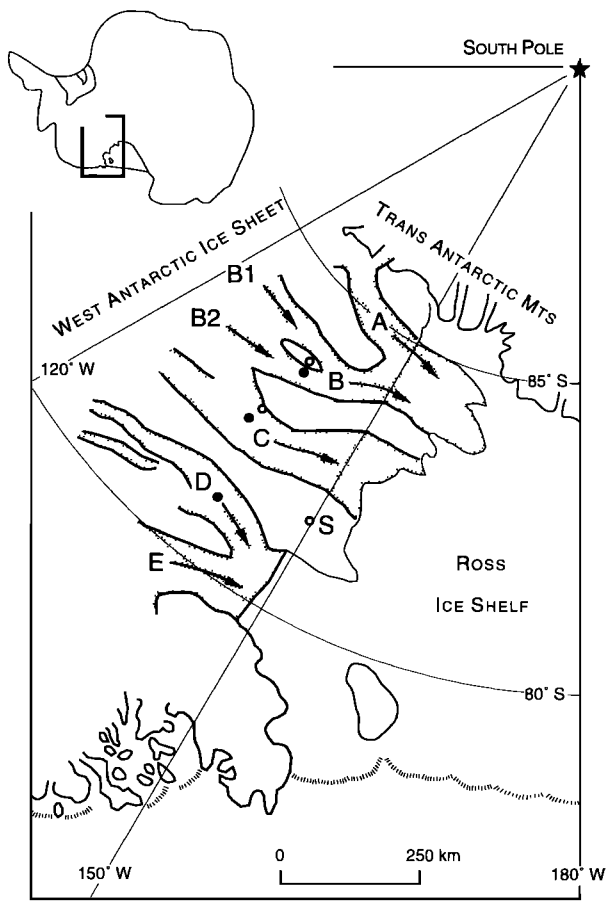

Figure 1. Sketch map showing West Antarctic ice streams (stippled) and location of study sites (solid dots on ice streams, open dots on interstream ridges and marginal shear zones). Arrows indicate the general ice flow. Ice streams are labelled A, B, C, D, E. These letters are placed so as to identify the study sites, from south to north as follows:
B, solid dot: Up B and New B
B, open dot: Unicorn (Ridge B1-B2)
C, solid dot: Up C
C, open dot: borehole 96-12, in shear margin of C.
D, solid dot: Up D
S, open dot: Siple Dome (Ridge C-D)

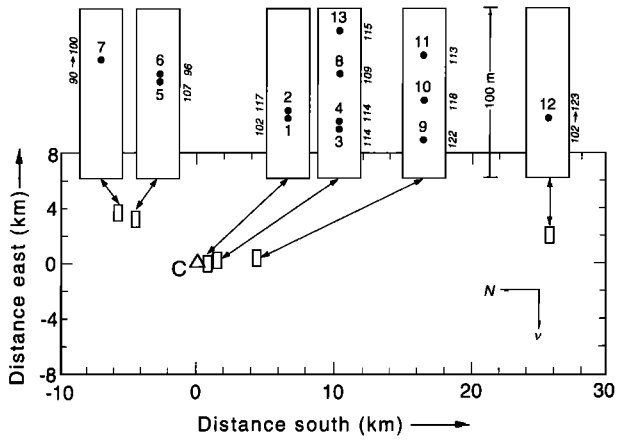

Figure 2. Map of the study site area on Ice Stream C, showing location of individual boreholes (black dots, identified by borehole number, with the prefix "96" omitted). On main map, in lower part of figure, locations of clusters of boreholes are shown schematically with small rectangles. Boreholes in each cluster are shown in strip maps (large rectangles) inserted along top of main map. Each strip map corresponds to a small rectangle on the main map via a two-headed arrow. Actual length of area shown in each strip map is 100 m as indicated. Italicized numbers along the sides of the strip maps give the water-level depth (in meters) in each borehole upon completion of breakthrough (Table 1). Major changes in water level are indicated with small arrows. Open triangle at origin of distance coordinate system is camp Up C, located at latitude 82° 26.5′ S, longitude 135° 58.0′ W. The arrow labeled *v* is the general westerly ice-flow direction in Ice Stream C.

The basal water pressure is measured in boreholes that have made hydraulic connection with a basal water-conduit system (see Section 7.1). During borehole drilling and for several hours after reaching the bed, the pressure measurements are made by measuring the depth of the borehole water level with a sounding float or by means of a pressure transducer placed at a depth of about 120 m in the borehole. Thereafter in some of the holes a pressure transducer is placed at the bottom, where it measures the basal water pressure directly. After the borehole freezes up and pressure transients have died away, and after sufficient time has elapsed for equilibrium between the sediment pore-water pressure and the pressure in the local basal water system, the pressure reported by the transducer represents the pore pressure. The pore pressure thus may manifest itself in long-term records of basal water pressure.

Ice overburden pressure is here estimated by calculation from an assumed ice density as a function of depth (E&K, Section 4). As a check, it can be measured by enclosing the pressure entry port of the transducer in an antifreeze-filled rubber gland (to prevent formation of ice inside the transducer body) and placing the transducer ca. 1 m above the bottom, where it comes to bear the ice pressure after the borehole has frozen up and the resulting pressure transients have relaxed. This check was made in borehole 93-9. The measured and calculated ice pressures agree to within about 0.4×10^5 Pa, the calculated pressure being the higher of the two (E & K, p. 213). For the other boreholes the ice pressure was obtained by the same type of calculation, with the ice density profile held fixed relative to the ice surface. A possible systematic error of 0.1 to 0.6 $\times 10^5$ Pa in these calculated pressures is indicated by the comparison for hole 93-9.

Basal water pressures are reported and discussed here mostly in terms of the equivalent borehole water-level depth below the ice surface; a 10 m increment in water level corresponds to a 1.0 bar (10^5 Pa) increment in water pressure. In general the "post-breakthrough water-level depth" given in Table 1 for each borehole is the deepest level recorded within several hours after the borehole makes connection. The water-level depths have a conservatively estimated accuracy of ± 1 m (E & K, p. 209). Ice overburden pressure is expressed in terms of flotation level, which is the water level that produces a basal water pressure equal to the ice overburden pressure.

Results of the pressure measurements (Table 1) are as follows. Outside the ice streams, boreholes do not make hydraulic connection with a basal water system, and no meaningful basal water pressure can be measured. In the ice streams, boreholes almost invariably make hydraulic connection with a basal water system (Section 7). The pressure in the system corresponds to borehole water level depths mostly in the range 100-115 m, with extreme values 96 and 123 m. Ice overburden pressures, calculated as explained above, correspond to flotation level depths in the range 98-101 m in Ice Stream B, 103-113 m in Ice Stream C, and 103 m in Ice Stream D. These figures show that the basal water pressures are in general quite high, close to the ice pressure—a situation that can result in significant enhancement of basal sliding and/or basal sediment deformation. This is best considered in terms of effective pressure—the difference between ice overburden pressure and basal water pressure, whose value in bars (10^5 Pa) is readily obtained from the difference between water level depth and flotation level depth (in meters), times 0.1. Basal effective pressures in Ice Stream B are mostly in the range –0.2 to +1.2 bar, with extreme values –0.3 and +1.6 bar; In Ice Stream C they are mostly in the range –0.9 to +1.1 bar with extremes –1.0 and +1.7 bar; and at the one site (with four boreholes) in Ice Stream D the effective pressure is uniform at + 0.4 bar. The mean effective-pressure values and standard deviations of the individual values about the means are +0.6 ± 0.6 bar for Ice Stream B, + 0.2 ± 0.7 bar for Ice Stream C, and +0.4 ± 0.0 bar for Ice Stream D. These mean values of effective water pressure

Table 1. Boreholes to Bottom in Ice Streams B, C, and D, and on Ridges B1-B2 and C-D; Water-Level Depth Before and After Breakthrough; Flotation Level and Basal Effective Pressure P'; Water-Level Drop Time (WLDT) and Time Constant T

Study site	Borehole Year-No.	Hole depth m	Water-level depth pre-breakthrough m	Water-level depth post-breakthrough m	Flotation level depth m	P' 10^5 Pa	WLDT min	T min
Up B	88-1	1035	-[a]	102	99	+0.3		
	2	(1035)[b]	-	111	(99)[b]	+1.2	540[q]	
	3	(1035)	-	105	(99)	+0.6		
	5	(1035)	-	109	(99)	+1.0		
	6	(1035)	-	115	(99)	+1.6		
	89-1	1058	-	113	101	+1.2		
	2	(1058)	-	115	(101)	+1.4		
	3	(1058)	-	112	(101)	+1.1		
	4	1057	-	99	(101)	–0.2		
	5	1057	28	98	(101)	–0.3	2	1.6
	6	1057	28	98	(101)	–0.3	3	2.7
	91-1	1055	-	112	101	+0.7		
	2	(1055)	-	108	(101)	+0.7		
	3	(1055)	16	109	(101)	+0.8	3	2.9
	92-1	1052	85	117	101	+1.6		
	2	(1052)	-	115	(101)	+1.4		
	4	(1052)	-	112	(101)	+1.1		
Unicorn	93-9[r]	910	30	30[g]				
	10[r]	914	24	29[g]				
	12[s]	993	38	39[g]				
	14[t]	1,092	30	30[g]				
New B	95-1	1,026	29	99	98	+0.1	2	1
	2	≈1026	82	96	-98	–0.2	5	6.4
	3	1,025	107[c]	107[d]	98	+0.9[l]	-	
	4	≈1029	21	98	-98	0	7[f]	
	5	1,028.5	22	100[m]	-98	+0.2	2.5	1.1
	6	1,029.5	62	97	98	–0.1	2	1.7
	7	1,026	33	105	98	+0.7	3	2.5
	8	1,027	51	104	98	0.6		
Up C	96-1	1,189	33	102	111	−0.9		
	2	-1,189	71	117	111	+0.8	2	2.6

Table 1, continued

Study site	Borehole Year-No.	Hole depth m	Water-level depth pre-breakthrough m	Water-level depth post-breakthrough m	Flotation level depth m	P' 10^5 Pa	WLDT min	T min
Up C	96-3	1,184	111[c]	114	111	0.3		
	4	-1,184	40	114	111	+0.3	2→30[h]	1.9[h]
	5	1,116	33	107	105.5	+0.15	15	10
	6	-1,116	37	96	105.5	–1.0	15	7
	7	1,088	27	90→100	103	–0.3	6[p]	1.4[p]
	7[i]	-1,088	65	107	103	–0.3	40[p]	6.5[p]
	8	(1184)	39	109	(111)	–0.2	5	2.3
	9	1194	58	122	111	+1.1	1.3	2
	10	1198	31	118	111	+0.7	2	1.3
	11	1201	55	113	111	+0.2	6	2
	12	1124	32	102→123	106	+1.7	~300[h]	75[h]
	13	1205	36	113	113	0.0	~2	3.3
Siple[u]	97-1	1004	-	-[g]				
	2	955	-	-[g]				
Up D	98-1	(1086)	120	107	(103)	+0.4	3[k], 2[n]	
	2	1086	87	107	103	+0.4	1	
	3	(1086)	54	107	(103)	+0.4	1	0.6
	4	(1086)			(103)			
	6	1,086	35	107→105	-103	+0.2	1.4	

a A dash in this column means that water level was not recorded but was generally in the range 20-30 m depth.
b Parentheses are used where an estimate of hole depth or flotation level is assumed to apply to nearby holes.
c Water level pumped down to this depth by the time the drill reached bottom.
d Water level remained at this depth after the drill reached bottom.
e This level was reached 36 min. after drill reached bottom; water remained at this level for 24 min., then began to rise.
f Estimated from measured drop rate from 20 to 47 m depth, extrapolated to 98 m.
g No breakthrough evident
h Complex drop curve; T value applies only to initial part.
i Redrilling of hole 96-7 after original hole lost connection to basal water system.
j Borehole at center of fossil marginal shear zone of Ice Stream C.
k Rise time (see Section 7.1).
l Valid if hole 95-3 did not bottom in frozen till (Sections 4.5 and 7.1). Not included in average effective pressure.
m After 1.7 days; initial level was 97 m.
n Drop time, after initial rise.
p Non-exponential drop curve causes large discrepancy between WLDT and T
q Water level dropped after a 9 hour delay.
r Station "Dragon Drill Pad" at edge of Unicorn (Ridge B1-B2)
s Station "Staging Area" between r and t
t Station "Fish Hook" near center of Unicorn
u Siple Dome, on Ridge C-D.
→ Indicates a change with time.

Figure 3. Photo of drill rig. From right to left the main components are: computer/personnel shelter, derrick, capstan, water-well pump winch (in front), four drilling-hose spools, eight water heaters, four high pressure pumps, two power plants, two snow-melting tubs (in front). Photos by H. Engelhardt.

are the lowest that have been reported for glaciers in which extensive pressure measurements have been made [*Kamb et al.*, 1994, p. 15,232]. Since the usually assumed basal sliding laws and till deformation laws [see e.g. *Bentley*, 1987; *Kamb*, 1993, pp. 28 and 71; *Kamb*, 1991, p. 16,585] predict basal shear motion increasing without limit as the effective pressure goes to zero under given basal shear stress, it stands to reason that rapid basal motion due to basal sliding and/or the shearing of basal sediments should be expected in the ice streams.

In Ice Stream B the pore water pressure in the basal sediment (Section 4), obtained from long-term water-pressure records and expressed as a borehole water-level depth, appears to lie mostly in the range 98-112 m (E & K, Figure 8), similar to the depth range 100-115 m quoted above for water levels observed shortly after borehole completion. Similarly, for Ice Stream C a two-year water pressure record (1997 and 1998) from borehole 96-8 (Figure 5) shows water-level depth varying over the range from 109 to 116 m. Thus the above expectation of water-

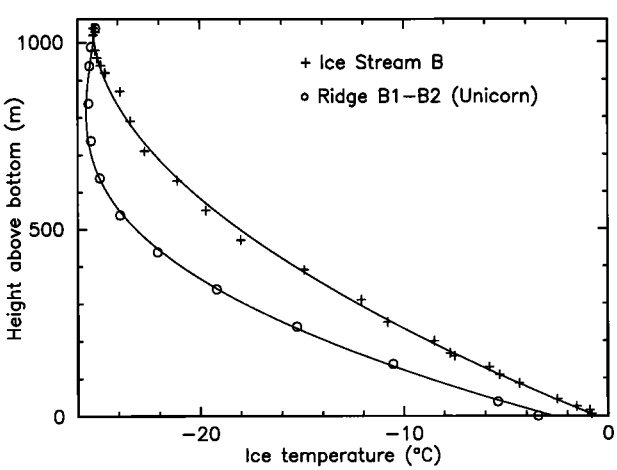

Figure 4. Vertical profiles of ice temperature in Ice Stream B (crosses) and in Ridge B1-B2 (circles). The Ice Stream B profile is near camp Up B, and the Ridge B1-B2 profile is at "Fish hook Station" (borehole 93-14). The smooth curves are fourth-order polynomial functions of depth, fitted to the temperature data.

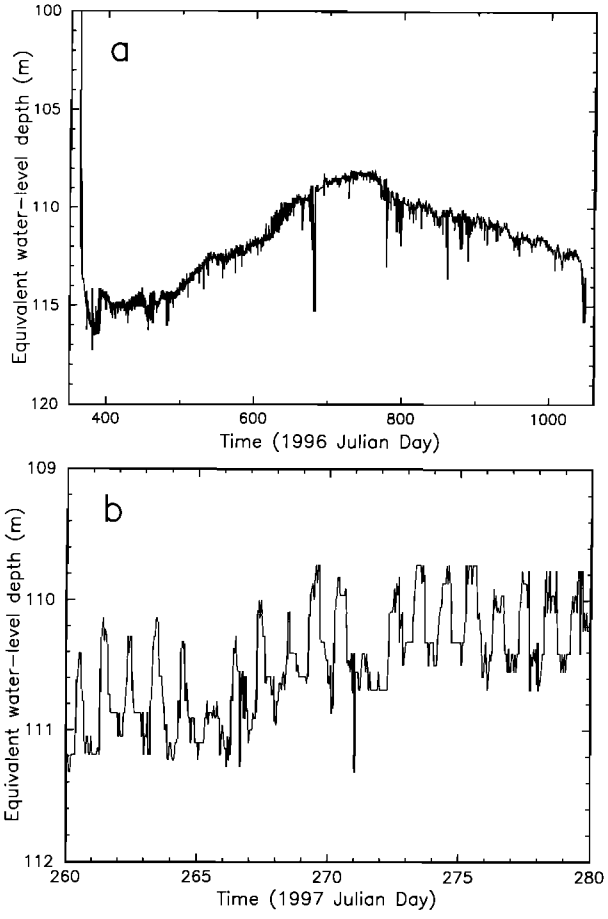

Figure 5. (a) Two-year record of basal water pressure under Ice Stream C (borehole 96-8). (b) Enlargement of a portion of (a), showing diurnal pressure fluctuations.

pressure enhancement of basal sliding and sediment shear seems to be generally valid whether pressure in a basal water system or in the pore water of the sediment is considered.

At times in the long-term water pressure records there occur periods of diurnal fluctuations in pressure, illustrated for Ice Stream C by Figure 5b and for Ice Stream B by E & K, Figures 12 and 13.

The cause of the pressure variations in Figure 5 is not known.

In summary, the basal melting of the ice streams makes basal sliding and bed deformation possible, and the high basal water pressure, producing unusually low effective pressure, is favorable for high rates of sliding and bed deformation. Thus the temperature and pressure observations support mechanisms (2) and/or (3) for ice-stream flow.

Further details concerning the pressure measurements are given in Section 7 and in E & K.

4. BASAL MATERIALS AND STRUCTURE

Samples of subglacial material were taken or attempted by piston coring at the bottom of one or more boreholes at each study site. The cores are listed with their individual lengths in Table 2. Each core is given a number of the form "96-6" or "96-7-3", in which "96-6" or "96-7" is the borehole number (Section 2 and Table 1). The additional cipher, such as the "3" is this example, is added when more than one core was taken in the indicated borehole, and designates (in this example) the third core taken, in order of coring. The early piston cores (to 1992) are 4.3 cm in diameter, while the later ones are 5.6 cm. The 4.3-cm core tube was 4 m long, the 5.6-cm tube 3 m or, in a few cases, 1 m long. The length of the core was never limited by the length of the core tube. A few small samples were obtained by their adhering to borehole instruments as illustrated in Figure 6. All cores were kept in sealed containers to minimize water loss, were hand carried from McMurdo to Pasadena, and were there stored in a refrigerator at + 1 C.

4.1 Basal Till

In the ice streams (including Ice Stream C) piston cores are commonly obtainable from boreholes that reach the bed. Overall, about 70% of the coring attempts were successful in obtaining a core 0.2 m or more long. With one exception (from borehole 95-3), the cores from the ice streams invariably consist of dark gray, wet, very sticky, clay-rich diamicton that shows no grading, bedding, or other structure as seen by core x-radiographs, by visual inspection of cores in the clear plastic core tubes, and by visual inspection of sediment adhering to instruments that have been lowered into the diamicton in situ (Figure 6). The diamicton is practically unsorted, the particle size distribution (Figure 7) extending from clay size ($\leq$ 1 μm) to almost the largest pebble size that can enter the core tube. The largest clast found so far measures 5.5×3.5×2 cm. Evidence for larger clasts in the diamicton or underlying bedrock is the considerable mechanical damage sometimes suffered by the core cutter. The clasts consist mainly of crystalline rocks—mainly granites and other plutonics, granitic gneisses, and schists, with rare volcanics (3%); there are ~10% sedimentary rocks, mainly well indurated graywacke. Exotics include small pieces of coal, the fine-grained fraction of which sometimes gives a coffee color to turbid water above the core in the core tube. Also, one spheroidal marcasite nodule in gray phyllite was recovered. The clasts are matrix supported, and the matrix contains about 35% mineralogical clay. The matrix also contains diatoms and other microfossils of a mixture of

Table 2. Subglacial Till Cores from Ice Streams B, C, and D, and from Interstream Ridge B1-B2 (Unicorn)

Study Site	Core No.	Core length m	Study site	Core No.	Core length m
UpB	89-1-2	0.6[d]	NewB	95-6	0.25
	89-1-3	0.3[d]		95-7-1	1.0
	89-1-4	1.95		95-7-2	0.25
	89-3-6[c]	1.45		95-8	0.4
	89-6-7[c]	3.1	UpC	96-3	0.2
	89-6-8[c]	1.3		96-6	0.35
	92-1	2.85		96-7-1	0.2
Uni[a]	93-10	0.3[e]		96-7-3	0.25
Uni[b]	93-14	0.3[e]		96-8	0.2
NewB	95-1	3.0		96-9-1	0.05
	95-3-1	0.9[e]		96-10	0.3
	95-3-2	1.9[e]		96-12	0.7
	95-5-1	0.75		96-13	0.3
	95-5-2	0.25	UpD	98-2	0.85
	95-5-3	0.5			

a Unicorn, Station "Dragon Drill Pad".
b Unicorn, Station "Fish Hook"
c For cores from UpB '89, the last cipher of the core number is counted up in sequence.
d Core taken with split-tube corer.
e Sediment is size-sorted and graded.

ages ranging from Eocene to Quaternary [*Scherer,* 1991].

On the basis of these and other petrological characteristics, and despite the absence of certain indications of deformation typical of tills (Section 4.7), *Tulaczyk et al.* [1998, p. 490] conclude that the diamicton is a glacial till—a sediment that has been transported and deposited by glacier ice without detectable involvement of running water [*Dreimanis,* 1988, p. 34]. We will thus refer to it henceforth as till. This is in harmony with the assumption of *Alley et al.* [1986] and of numerous later authors. The till was probably derived from Tertiary glacimarine sediments of the Ross Sea sequence, whose sedimentological and petrologic features are similar [*Tulaczyk et al.*, 1998, p. 492], and which are inferred from seismic data to underlie the till with erosional truncation in the region of the West Antarctic ice streams studied here [*Rooney et al.*, 1987, 1991]. None of our cores recovered bedded and/or indurated sediment that could represent the inferred underlying sedimentary bedrock. The foregoing information is summarized from much more extensive presentations by *Tulaczyk et al.* [1998] and *Tulaczyk* [1999, Chapter 2].

The near complete lack of volcanic clasts in the till raises doubt as to the widespread occurrence of volcanic rocks in the catchment regions of Ice Streams B, C, and D, contrary to a widely held view [e.g. *Blankenship et al.*, 1993; *Behrendt et al.*, 1994].

The till is unfrozen and ice-free as the cores are brought to the surface. This confirms the conclusion from temperature measurements (Section 3.1) that the melting isotherm lies at the base of the ice.

The basal till is soft and deformable, and, as detailed below, it is water saturated. It thus corresponds rather well with the deformable basal till visualized by Alley et al. (1986) in their interpretation of seismic data [*Blankenship et al.*, 1986]. More information on till deformability is given in Section 6.

4.2 Water Content of Till

Measurements of the water-saturated porosity of the till, which is related to the till's strength and loading history (Section 6.5), are plotted in Figure 8 and summarized in Table 3. Porosities are determined by weight-loss on drying and are of two types: bulk porosity, which is the porosity of each sample as taken from the core, and matrix porosity, which is the porosity indicated by the weight loss measurements when all clasts greater than 4 mm in size are removed. Matrix and bulk porosities differ by 1-3%, as shown by the data in Figure 8b and Table 3. Mean porosities are nearly the same in Ice Streams B and C, about 40%, but the scatter of measured values is greater in C (Table 3). From seismic data from Ice Stream B *Blankenship et al.* (1987) inferred a porosity of 40%. Porosities in Ice Stream D (Figure 8b) are on average about 8% higher than in B or C, a considerable difference. This may be due to the fact that the Ice-Stream-D samples were better protected from water loss after core recovery, but it may also be related to the smaller strength of the Ice-Stream-D till (Section 6.1). The highest porosities are about as high as what is typically encountered in the most porous soils, with porosities up to about 45-50% [*Lambe and Whitman,* 1969, Table 3.2]. Particularly noteworthy is the high matrix porosity of 60% for the specimen at the top of core 98-2 (Figure 8b; Table 3, note 3). It may indicate some incorporation of water into the top of the core in the piston-coring process.

Figure 8b shows that for Ice Stream D there is a general decrease in porosity with depth below the top of the till, interrupted by a gentle peak in porosity at a depth of about

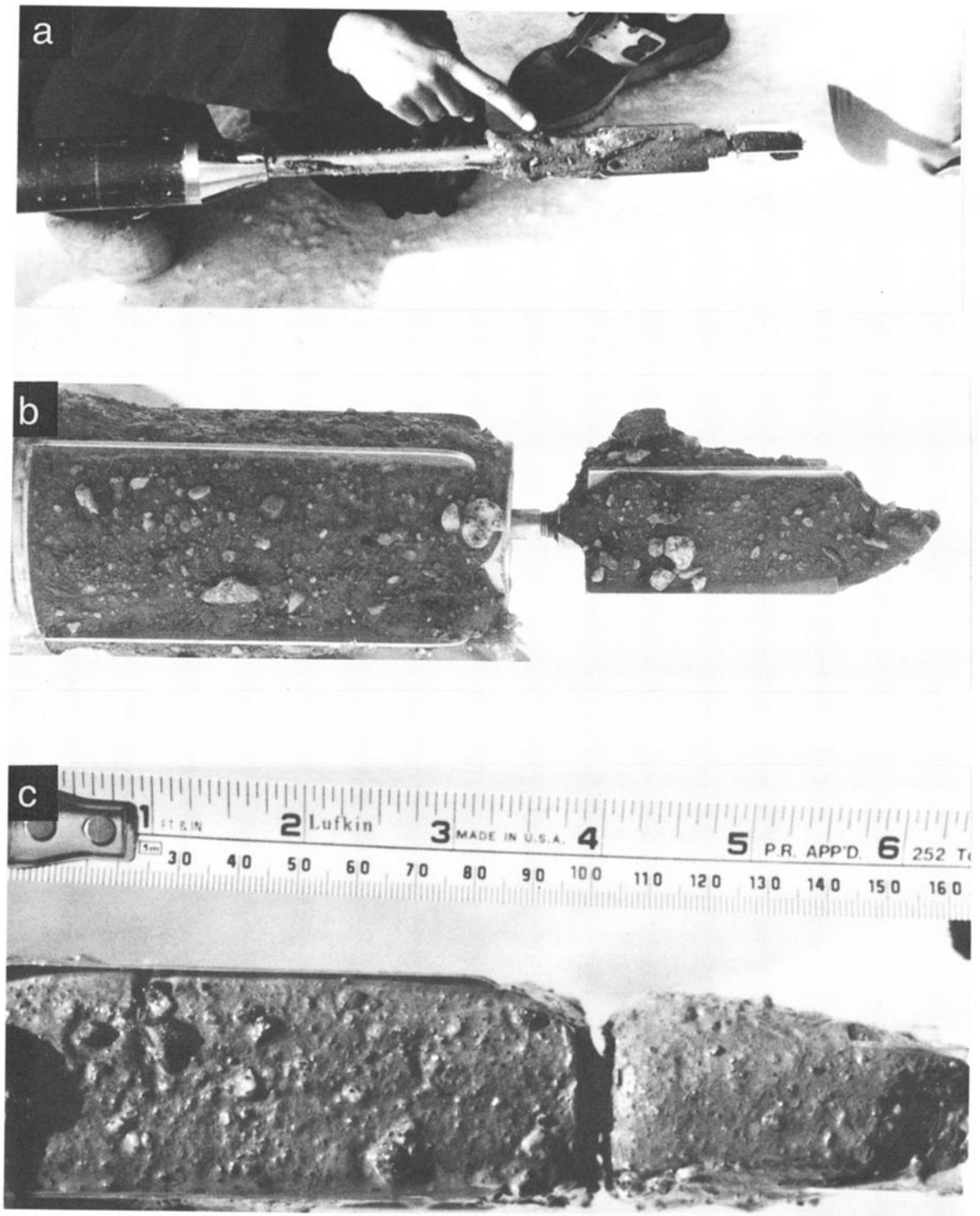

Figure 6. Photos of till adhering to torvane instrument. Instrument body is to the left, with main vane to the right, connected to the body by a 0.25-inch shaft, visible in (b). In (a) the scale is shown by the hand. In (b) and (c) the counter-torque vane is to the left. In (c) the till surface is wet, while in (b) the surface is freeze-dried. Photos by H. Engelhardt.

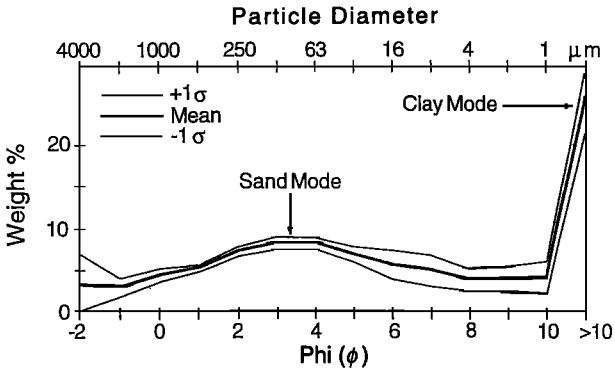

Figure 7. Particle size distribution in till, averaged from 35 till samples taken from 5 piston cores. Ordinate is weight percent of till solids per 1.0 phi interval. (Phi is minus the logarithm to the base 2 of the particle size in millimeters.) "Clay mode" is all particles smaller than 0.5 μm. σ is estimated standard deviation. From *Tulaczyk et al.* [1998, Figure 3A].

26 cm. Porosities of Ice-Stream-B till do not show a trend of this kind, except for the top two values from core 92-1 (Figure 8a). A decrease in porosity with depth is qualitatively what is expected due to the difference between the lithostatic and hydrostatic pressure gradients, which results in an increase in effective pressure from the top of the till downward. (The assumption of a hydrostatic gradient does not strictly apply if there is pore water flow in the vertical direction.)

The Atterberg liquid limit [*Lambe and Whitman*, 1969, p. 33], measured on a till matrix sample from Ice Stream B and expressed as a saturation porosity, is 42.5%. Although by this standard the measured porosities are quite high, there is no indication that the till approaches a slurry in its mechanical behavior.

The pore space of the till at depth, in-situ, is fully water saturated (see argument below). When the till is brought up from depth to the surface, some of the air that at depth was dissolved in the pore water exsolves, forming numerous small air-filled tubules ~1 cm long and ~1 mm in diameter within the till. Some of the tubules break through visibly to the core surface and emit bubbles of air. Many of them are aligned subparallel to the core axis and can be seen in x-radiographs of the core. Because of the air tubule content the cores tend to lengthen somewhat within the core tube and swell slightly on extraction from the core tube. As long as pore water from within a till specimen does not seep out of the till and get separated from the till in the air exsolution process, the in-situ water-saturated porosity measured by weight loss on drying will be unaffected by the exsolution.

In the triaxial tests (Section 6.3) a pore water pressure of $3.8\text{-}6.9\times10^5$ Pa (called the saturation pressure) is sufficient to eliminate the air bubbles in the pores of the till test specimens (Tulaczyk, 1999, Chapter 4, Appendix 4.A). The saturation pressures are so much smaller than the ambient hydrostatic pressure at depth (ca. 90×10^5 Pa) that complete water saturation of the till in situ is assured.

4.3 Thickness of Till

From seismic data *Blankenship et al.* [1987, p. 8907] interpreted the till at its discovery site near Up B as forming a basal layer 8.1 ± 0.3 m thick, and from seismic profiles *Rooney et al.* [1987, pp. 8915, 8918] judged the

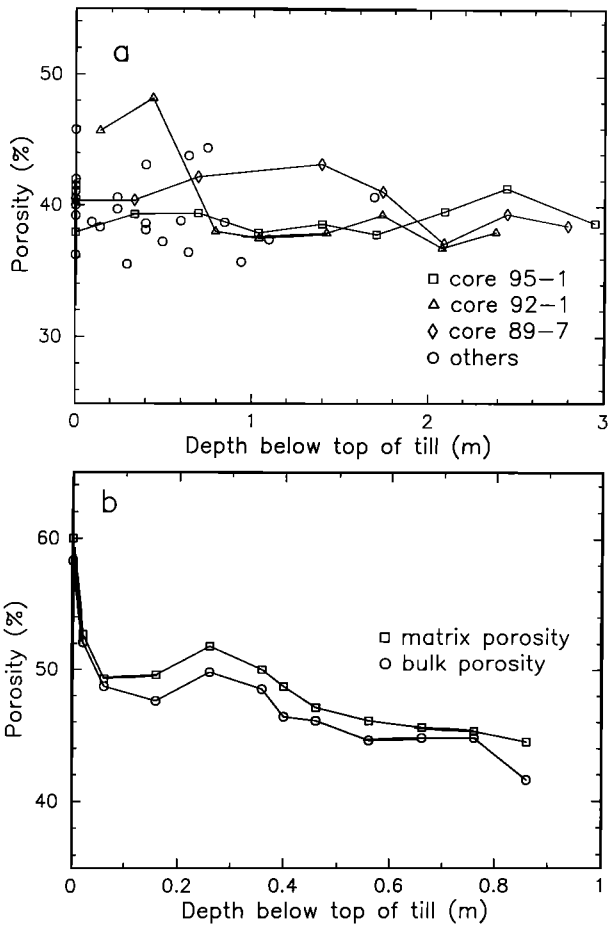

Figure 8. Porosity of till as a function of depth below the ice-till interface, (a) in Ice Stream B, and (b) in Ice Stream D. (b) shows both bulk and matrix porosities, while in (a) only matrix porosities are shown. In (a), the core designated 89-7 is the one labelled 89-6-7 in Table 2.

Table 3. Summary of Measured Till Porosities

Ice Stream	Type	Range %	Mean %	s.d. %	s.d. of mean %	No. of samples	Depth range (m)	Notes
B	matrix	33-44	40	3	0.5	48	0-3.0	1
C	matrix	28-60	42	7	1.5	19	0-0.35	2
Cm	matrix	45-52	48	4	2	5	0-0.7	3
D	matrix	44-53	48	3	1	11	0.02-0.8	4
C	bulk	26-58	40	8	2	19	0-0.35	2
Cm	bulk	44-52	47	4	2	5	0-0.7	3
D	bulk	41-50	46	3	1	11	0.02-0.8	4

1. Data of Figure 7a, from Up B and New B.
2. Unpublished data.
3. "Cm" means marginal shear zone of Ice Stream C, core 96-12.
4. Data of Figure 7b. Omits sample from depth 0, of bulk porosity 58%, matrix porosity 60%.

layer to vary in thickness from 13 m to zero (or to the minimum seismically resolvable thickness of 2 m). The lengths of the till cores (Table 2) represent minimum till thicknesses—minimum because the piston corer is subject to being stopped prematurely by running into large rock clasts in the till. The minimum till thickness for Ice Stream B near Up B is about 3 m, except in the "till-free swath" (Section 4.4), where the minimum is about 0.7 m. For Ice Stream C the minimum is about 0.3 m, except in the fossil marginal shear zone (borehole 96-12), where it is 0.7 m. The core lengths are probably more a measure (inversely) of the concentration of large clasts in the till than of the thickness of the till layer.

On several occasions, drilling tests in the till were carried out to see if the water-jet drill could penetrate detectably to the bottom of the till and reveal its thickness. This might be possible if the underlying sedimentary "bedrock" (Section 4.1) is sufficiently indurated to be detectably less penetrable than the till. A test on the Caltech campus, in which the water jet was used to drill down into alluvial sand and gravel, achieved a penetration of 5.5 m in 30 minutes of drilling time, showing that penetrations of this order are achievable. Tests in ice-stream boreholes seem to indicate drill penetrations of 5 to 15 meters, without an indication that the drill reached the bottom of the till in any of these holes (hence the apparent drill penetrations are minimum apparent till thicknesses.) The apparent penetrations of 5-15 m are much larger than those achieved by other means—up to 3 m by piston coring (discussed above) and up to 0.7 m by slide-hammer penetrometer, tethered stake (Section 5), and torvane (Section 6), based on till coatings on them (Figure 6). Such coatings are generally not present on the hot-water drill stem, but in one rare case (borehole 95-4) the drill had a till coating up to 1.1 m above the tip. The coatings give only a minimum penetration because of their tendency to be washed off in the process of hauling the instruments to the surface.

The above results suggest a till thickness varying from ~0.5 to ~10 m, and are compatible with the 6.5-m average thickness inferred by *Rooney et al.* [1987, p. 8918] from seismic data.

4.4 Search for Till-free Bed

On Ice Stream B the L2 and L3 seismic profiles of *Rooney et al.* [1987, p. 8918] are inferred by these authors to cross a 300-m-wide swath of the bed over which the till layer is either absent or is thinner than the seismic resolution of 2 m. To test the ability of borehole observations to confirm the seismic interpretation, four boreholes were drilled on the original position of profile L2 and near the center of the swath (holes 95-3, -4, -5, -6); also two boreholes (95-7, -8) on its north flank where the

till should be thin but not absent according to the seismic profiles. Borehole 95-3 behaved in a very peculiar way as discussed in Section 4.5, whereas boreholes 95-5 to -8 yielded till cores of normal lithology, showing that till is not absent. The till cores from the swath (95-5-1, -2, -3, and 95-6) are rather short, 0.2-0.7 m (Table 2), suggesting that the till is thin (~0.7 m) in the area sampled. Hole 95-4, which was about 12 m from holes 95-5 and 95-6, penetrated the till to the depth of at least 1.1 m as noted in Section 4.3, so the minimum till thickness in the swath center must be taken as 1.1 m despite the shorter cores. Drilling penetration tests of the kind discussed in Section 4.3 indicated an apparent minimum till thickness of 10 meters in borehole 95-6, at the swath center, and 16 meters in hole 95-7, on the north flank. The cores from the north flank (95-7-1, 95-7-2, 95-8) have a range of lengths 0.25-1.0 m (Table 2), similar to the cores from the swath center. In these till thickness data there is not a clear distinction between center and flank, contrary to what is portrayed in the seismic section.

4.5 Frozen Till

Boreholes outside the ice streams, in particular on Ridge B1-B2 (the Unicorn), bottom in frozen till. This is established as follows. The boreholes yield basal sediment cores, which are very different from the till cores from the base of the ice streams. The sediment is a diamicton of mineralogical/petrological/paleontological characteristics similar to the Ice Stream B till, except that it lacks most of the clay component that is so abundant in the till, and it is sorted and graded, fining upward from pebbles at the bottom to fine sand and silt at the top. These characteristics, together with the sub-freezing basal temperatures (Section 3.1), indicate that prior to drilling, the sediment occurs frozen in the ice, and is melted out of the ice by the hot-water drill. The water jet blasts the finer particles into suspension, from which they then settle out in the borehole, producing the sorting and grading. Clay is mostly winnowed out of the sediment column as sampled a few hours after drilling, because the settling velocity of the clay particles is small. A repeated cycle of attempted drilling followed by piston coring yields additional sediment of similar characteristics. It appears that the drill cuts slowly down into frozen, ice-saturated till, and also melts out sediment particles from the borehole wall. The advance of the drill is slowed and finally stopped by the accumulation of large rock clasts in the hole, too large to be blasted out of the way by the water jet or picked up in the core barrel. Another sign of drilling into frozen till is numerous fresh scratches along the length (4 m) of the brass drill stem, especially along the lowermost 1 m.

The available borehole observations do not provide a sufficient basis for distinguishing an abrupt from a gradational contact between frozen till and clean ice, or for recognizing the presence of a moderate amount of rock debris in the ice overlying the frozen till. (A heavy loading of debris would constitute essentially frozen till.) Observations of the slowdown in drilling speed as the bottom is approached, somewhat like the observations presented in Section 7.7 might allow these distinctions to be made.

At Siple Dome, on Ridge C-D, the bed appears to be solid bedrock without overlying till. About 0.1 kg of fine sediment was recovered from just above the bed in a sediment trap carried by the hot-water ice-coring drill. In the lowermost 30 cm of the deepest ice core, just above the bottom, a few small (~1 cm) rocks were found imbedded in the ice. Only a small amount (~ 1 cm^3) of sediment was recovered by the piston corer, which was heavily damaged by impact with solid rock(s).

The difference between the development of frozen till under Ridge B1-B2 and the lack of till development under Ridge C-D may be related to evidence of former streaming movement in Ridge B1-B2 and the lack of such evidence for Ridge C-D (H. Engelhardt, personal communication, 1999). The implication is that ice-stream motion is necessary to generate basal till, as is generally thought [*Cuffy and Alley*, 1996].

Surprisingly, the behavior of borehole 95-3 in Ice Stream B was quite similar to the Ridge B1-B2 boreholes both in terms of basal sediment cores as described above and in terms of the lack of breakthrough to a basal water system (Section 7). Hole 95-3 thus appeared to have bottomed in frozen till, contrary to the overwhelming expectation from drilling experience in the ice streams (E & K, p. 210). Boreholes only 3.5 and 7 m away (95-4, 95-5, and 95-6) bottomed in wet unfrozen till in what seemed the normal manner. However, details of the drilling records discussed in Section 7.7 imply that holes 95-4 and 95-5 penetrated through a thin frozen till layer and into normal unfrozen till below, indicated by piston cores. It seemed that the mass of frozen basal till that apparently stopped the drill in hole 95-3 became progressively thinner (or less debris-rich) as traced laterally past holes 95-4 and 95-5, where it slowed but did not stop the drill.

An alternative to the foregoing interpretation of borehole 95-3 is given in Section 7.1.

If the ice is frozen to the bed in the vicinity of hole 95-3, a sticky spot [*Alley*, 1993] would be expected there on the basis of Section 3.1. A similar expectation might be entertained if the till layer were absent in the "till-free swath" (Section 4.4). But no indication of a sticky spot

has been found in this vicinity, either by flow-velocity measurement [*Whillans and van der Veen*, 1993; *Hulbe and Whillans*, 1994] or from basal microseismicity such as that observed in Ice Stream C [*Anandakrishnan and Bentley*, 1993]. A few microearthquakes were observed in Ice Stream B, but not near borehole 95-3.

In the expectation that the till might be absent or the bed might be frozen in the zone of microearthquake activity in Ice Stream C, boreholes 96-5, -6, and -7 were drilled at two sites where clusters of microearthquake epicenters had been located by *Anandakrishnan and Bentley* [1993]. However, these boreholes revealed normal ice-stream basal conditions—an unfrozen bed with till present. This might be explained by the seismic interpretation of *Anandakrishnan and Alley* [1994] that the probability that a randomly located borehole will hit a sticky spot is $\sim 10^{-3}$.

A recently measured flow-velocity profile across Ice Stream C [*Engelhardt*, unpublished data] reveals that the microearthquake zone lies at the southern edge of a large sticky area, ~10km x 20km in dimensions, which is shown also by a satellite image [*Engelhardt*, unpublished data] and a radar profile of basal topography and ice layering [*Conway et al.*, submitted, 2000]. Whether the microearthquakes occur at "stickier spots" within the sticky area remains to be seen.

4.6 Relation of Till and Bedrock to the Melting Isotherm

The presence of frozen till at the base of the ice sheet implies a thermally layered basal zone in which cold glacier ice overlies frozen till which in turn overlies either unfrozen till or bedrock, frozen or unfrozen, depending on the location of the melting isotherm relative to the till/bedrock contact. When a borehole terminates in frozen till, the drill falls short of reaching the melting isotherm. The basal temperature that is measured is the temperature at the depth reached by the drill, but the mechanically most significant level is the base of the frozen till, where the temperature is at the freezing point if unfrozen till underlies frozen till, or below freezing if frozen till directly overlies frozen bedrock. In the latter case there will be no appreciable basal sliding or till deformation, whereas in the former case the base of the frozen till will probably act as the glacier sole in any basal sliding that occurs and will be the upper limit of any shear zone that forms in the unfrozen till below. This seems to be the situation at boreholes 95-3, -4, -5, and -6, as discussed in Section 4.5. In the ice streams (except at these boreholes) thermal layering of the basal zone appears always to be simply cold ice over unfrozen till over bedrock, so that the basal temperature measurement always gives the pressure melting point or a value close to it. But in the ice sheet of Ridge B1-B2 there is a thickness of frozen till sufficient to stop the drill before it reaches the melting isotherm, so that sub-freezing basal temperatures are measured (Section 3.1). "Basal" here refers to the bottom of the boreholes rather than the base of the frozen till. From these basal temperatures we can calculate an estimated depth of the melting isotherm beneath the bottom of each borehole by assuming that the vertical temperature profile measured just above the base (as in Figure 4) continues downward with unchanged thermal gradient. For the four temperature profiles in the Unicorn the results are 10, 10, 24, and 41 m. If the total thickness of till (frozen, plus unfrozen if any) is 6.5 m, which is the average thickness estimated from seismic data (Section 4.3), and if the thickness of frozen till penetrated by the drill in each hole was ~1 m, as estimated from the total length of piston core recovered from each hole (Table 2), then these figures indicate that the ice sheet is in fact frozen to the bed there. At Siple Dome (basal temperature –2.35 C) the estimated depth of the melting isotherm beneath the bottom of the borehole is 56 m, by the same type of calculation. Thus even if, contrary to the interpretation in Section 4.5, there were a ~10 m thickness of till beneath the bottom of the hole, the till would be frozen and the ice sheet would be frozen to the bed. These results substantiate the conclusion in Section 3.1 that the ice sheet outside the ice streams is frozen to its bed.

As noted earlier (Section 3.1), in Ice Stream C the measured basal temperature, from boreholes 96-2 and 96-12, is 0.35 degrees C below freezing, which by the above reasoning indicates a melting isotherm 7 m below the depth level reached in the boreholes. This allows a frozen or unfrozen bed, depending on whether the bedrock lies less than or more than 7 m below the bottom of the boreholes.

If the indication of 0.3-m till thickness (Section 4.3) is correct, then Ice Stream C would appear to be frozen to its bed, which would account for the cessation of its streaming motion (Section 2). However, this conclusion is contradicted by the fact that only piston cores of unfrozen till were obtained from the boreholes in Ice Stream C (Table 2), and by the fact that all deep boreholes in Ice Stream C made connection with a basal water system (except possibly hole 96-3: see Section 7.1). This situation is considered further in Section 8.2. Geophysical evidence for an unfrozen bed under Ice Stream C is summarized by *Anandakrishnan et al.* [2000].

4.7 Lithologic Evidence re Till Deformation

Structural features indicative of soft-sediment deformation are found in many northern-hemisphere tills that are thought to have lubricated the motion of the

Laurentide and Scandinavian ice sheets [*van der Meer*, 1993], and such structures would be expected in till of the Antarctic ice streams if the till-lubrication model of the ice-stream mechanism is valid. A search has been made of the core-x-radiographs, individual till clasts, and till thin sections in an effort to identify lithologic and structural features produced by till deformation.

In the ice-stream till cores a vertical preferred orientation of the larger clasts is seen in radiographs, whereas a horizontal preferred orientation would be expected for extensive shear across horizontal planes. There is also in general a pronounced vertical orientation of the air-filled tubules (Section 4.2). These vertical preferred orientations are probably caused by a vertical extension of the till within the core tube as the air tubules form and expand. In core 89-4 the vertical orientation of the tubules and elongated clasts changes to horizontal within the upper 5 cm of the core, suggesting a horizontal planar anisotropic structure (planes of weakness) that would be expected for a zone of basal shear deformation in the till. Five more features of the same type, of thicknesses 2, 2.5, 6, 7, and 11 cm, have been found in cores 92-1, 95-5, and 95-7, but none of these are at the top of the core, which suggests that shear zones form at various depths in the till. However, the lack of microscopic evidence for such shear zones (see below) weakens their significance as evidence for till deformation.

Although evidence for subglacial comminution (i.e. clast crushing and abrasion) is not taken to be a criterion in the definition of till [*Dreimanis,* 1988, p. 34], such evidence is so common in tills that it is widely considered one of their most important distinguishing features [*Dreimanis,* 1990; *Harlan et al.,* 1966]. Striations are the most dependable indicator of clast abrasion [*Harlan et al.*, 1966] and are present on many clasts from North American Pleistocene tills [*Anderson,* 1955; *Drake,* 1972; *Holmes,* 1952]. But they are almost completely absent on clasts from the Ice-Stream-B till: only two clasts, 0.9%, showed (questionable) striations [*Tulaczyk et al.,* 1998, p. 489]. The clasts are mainly subangular to subrounded, and although rounding and rounded edges sometimes result from glacial abrasion [*Flint,* 1971, p. 165], it appears that in the Ice-Stream-B till they are associated with chemical-weathering features such as etch pits and therefore did not result from abrasion.

Extensive SEM examination of the surfaces of small (125-250 μm) clastic particles from the till has revealed that, contrary to what is typical in tills, there are very few microscopic features of particle fracture, crushing, grinding, abrasion, or comminution [*Tulaczyk et al.,* 1998, p. 491]. The few recognizable features of this kind are generally overprinted by features of chemical weathering, which might be taken to imply that a long period of weathering has intervened since the last recorded deformation of the till. A grain-scale indication of current or recent till deformation is thus lacking.

Thin sections of impregnated till that was not disturbed in core sampling show no discrete shears or other visible macroscopic or microscopic fabric suggestive of deformation. Clay particles are aggregated into thin, microscopically visible "plasma", which show no preferred orientation in the till matrix, contrary to what is expected as a manifestation of till deformation. Some of the plasma conspicuously coats the surfaces of the clastic grains (mainly quartz and feldspar). Such grain coatings are called "skelsepic plasmic fabrics" by *van der Meer* [1993, p. 555 and Figure 5] and are attributed by him (p. 559) to "rotational deformation", which he explains as follows: "A deforming till bed may be regarded as consisting of stacked, rotating wheels" of the till sediment [*van der Meer,* 1997, p. 828 and Figures 3 and 4]. If that concept is valid, and if "rotational deformation" can be related mechanistically to development of the plasmic coatings on grains and to the till lubrication process, one may be able to recognize the coatings as evidence for till deformation and therefore modify the first sentence of this paragraph.

Definite lithologic evidence for till deformation is present in the mixing of diatom ages in the till (Section 4.1), which requires some kind of stirring action that involves till deformation. The relative scarcity (by a factor ~10^3) of whole diatoms in the Up B till by comparison with glacimarine sediments of the Ross Sea may be an indication of mechanical disintegration of the fragile diatom tests by till deformation, but it could also result from chemical weathering [*Tulaczyk et al.*, 1998, p. 491].

Although lithologic evidence for till deformation is thus mostly lacking, evidence of other kinds (Sections 5 and 6) is fairly convincing that till deformation plays a role in the ice-stream mechanism. The lack of lithologic evidence is taken as an indication of the validity of the hypothesis that the subglacial deformation of clay-rich till produces no significant particle comminution because of a "cushioning" action of the clay-rich matrix, which is particularly likely under low effective pressure [*Tulaczyk et al.*, 1998, pp. 493-494].

5. BASAL SLIDING VS. TILL DEFORMATION

Since physical conditions at the base of the ice streams favor both basal sliding and till deformation as mechanisms for rapid ice-stream motion (Section 3), measurements are needed to evaluate observationally their actual

contributions to the ice stream motion. This is important for any predictive models of ice stream behavior because the till flow law and the basal sliding law are probably quite different. We have made two measurements of basal sliding (and indirectly of till deformation), one on Ice Stream B (borehole 95-1) and one on Ice Stream D (borehole 98-3). The method of measurement (called the "tethered stake") and the results for Ice Stream B are given by *Engelhardt and Kamb* [1998].

These results indicate that at the New B site, sliding contributed 80% to 100% of the total motion over an observational period of 22.5 days, which was interrupted by a 3.5-day period of slow apparent sliding (8% of the full motion). From certain details in the sliding-vs.-time curves, *Engelhardt and Kamb* [1998, p. 228] concluded that the slow apparent sliding was an artifact caused by the tethered stake getting temporarily caught on rock clasts protruding from the ice sole. Even if this conclusion is incorrect, the average basal sliding motion is still large, 67% of the full motion. This sliding motion is basal sliding *sensu lato*: it is the sum of any sliding across the ice-till interface (sliding *sensu stricto*) plus any till shear from the top of the till down to the level of the tethered stake, which *Engelhardt and Kamb* [1998, p. 227] estimate to have been only about 3 cm below the sole. These results seem to indicate a dominant role for basal sliding in ice stream motion, or else they indicate that if till deformation dominates the motion, it is concentrated in a narrow shear zone at the top of the till and not distributed uniformly through the ca. 5-m inferred thickness of the till layer (Section 4.3), as has commonly been assumed.

In the last 2 days of tethered-stake observation at the New B site the measured apparent sliding reached 1.17 m d^{-1}, essentially 100% of the full ice-stream motion. This implies not only that the till-deformation contribution to the motion was zero, but also that there was a negligible contribution from ice deformation. This rules out enhanced ice deformation (Section 1, item (1)) as a mechanism of ice-stream motion, at least in this case. It is worthy of note since direct measurements of ice deformation that are needed to check mechanism (1) have not been made.

The basal-sliding results from Ice Stream D were obtained with a tethered-stake instrument improved over the original instrument in two ways: (1) it carries a greater length of tether line (300 vs. 21 m), which greatly increases the total amount of basal sliding that can be recorded; (2) the stake can be locked so that in a preliminary run the instrument can be lowered into the till without releasing the stake, and the depth of penetration into the till registered by the coating of till on the instrument. This was done in borehole 98-2. The depth of penetration of the bottom tip of the stake into the till was 63 cm, and the corresponding penetration of the tether attachment point at the top of the stake was 34 cm. The instrument with latch pins unlocked was then emplaced in the till at the bottom of hole 98-3, the stake was released, and its motion has been tracked continuously by the instrument and telemetered to Pasadena via the ARGOS data system since 22 January 1999. The record of apparent sliding distance with time (Figure 9) shows an initial apparent sliding speed of about 0.8 m d^{-1}, decreasing in a few days to about 0.2 md^{-1}, and decreasing gradually further to about 0.1 md^{-1} toward the end of March, with continued slow decrease thereafter. These speeds (except the initial 0.8 md^{-1}) are a small fraction of the surface velocity of 1.0 md^{-1} measured by GPS, and appear to indicate that most of the ice-stream motion is accommodated by till deformation below the level at which the tethered stake was emplaced (34 to 63 cm beneath the top of the till according to the preliminary run with the stake locked). A similar conclusion is reached by *Truffer* (1999, p. 38) for deformation of a 7-m-thick till layer at the base of Black Rapids Glacier, Alaska.

The relative amounts of till deformation inferred above for Ice Streams B and D do not correspond well with the till porosity profiles in Figure 8. The profile for D (Figure 8b), with a sharp, high peak in porosity at the top of the profile (depth = 0), giving a narrow zone of till weakness according to Section 6.5, should correspond to a narrow shear zone at the top of the till; but such a shear zone is a possibility inferred above from the tethered-stake data for Ice Stream B, not Ice Stream D. Except perhaps for profile

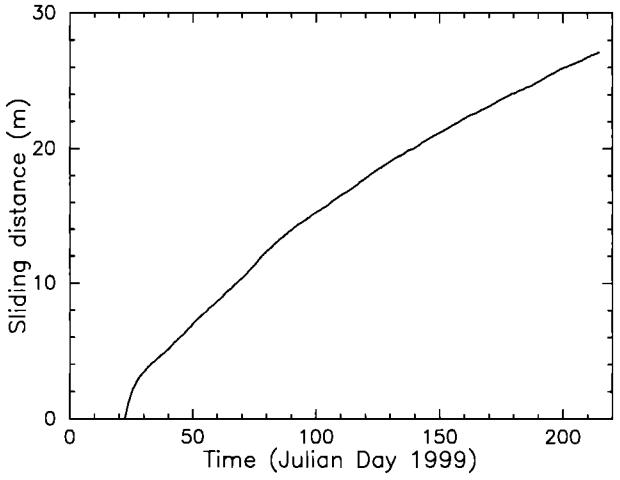

Figure 9. Displacement record for tethered stake in Ice Stream D, borehole 98-3. Pay-out of tethering line provides a measure of basal sliding (sensu lato). The slope of the curve is the sliding velocity.

92-1, the porosity profiles for Ice Stream B (Figure 8a) do not indicate a definite depth dependence of the till porosity and thus correspond better with the distributed till deformation inferred above from the tethered stake data for Ice Stream D, not Ice Stream B.

On the other hand, a concentration of till deformation close to the ice sole is compatible with a profile of till shear strengths from Ice-Stream-B cores (Section 6.2) and with an in-situ strength profile discussed in the last paragraph of Section 6.4.

The very contrasting results for Ice Streams B and D—basal sliding rapid and generally increasing with time in B, basal sliding slow and decreasing with time in D—illustrate the difficulty of making valid generalizations about the ice-stream mechanism with the amount of observational material so far in hand. The ratio of sliding to till deformation varies from one ice-stream site to another, and it appears also to vary with time. Until the problem of accounting for the amounts of basal sliding and till deformation is solved, we cannot consider the ice-stream mechanism to be understood.

6. TILL STRENGTH AND RHEOLOGY

Insofar as till deformation plays a significant role in ice-stream motion, the mechanical properties of the till are of much interest and importance. It has been generally assumed, following *Boulton and Hindmarsh* [1987, p. 9063], that the till behaves rheologically as a linear or slightly nonlinear viscous fluid [*Alley et al.*, 1987b; *Alley*, 1989b; *MacAyeal*, 1989, 1992; *Alley et al.*, 1989; *Hulbe*, 1998; *Hulbe and MacAyeal*, 1999]. However, since the till is a granular medium (Section 4.1) of composition and structure well within the range of granular media dealt with in soil mechanics, its rheological behavior should fall within the range exhibited by these materials. As such, it should show treiboplastic* (Coulomb-plastic) rheology: it should have a yield stress that is controlled by intergranular friction and that depends only slightly if at all on the strain rate [*Kamb*, 1991]. We have carried out four types of mechanical tests in an effort to resolve the question whether the till rheology is viscous or treiboplastic and to define its mechanical properties in relation to the contribution it may make to the ice stream mechanism.

Most of the tests were made on till samples obtained by piston coring. In order to provide information on the strength of the till in situ at the bottom of an ice stream ~1000 meters deep, the tests in Sections 6.1 and 6.2 depend on the "$\phi = 0$ concept" of soil mechanics [*Lambe and Whitman*, 1969, pp. 433, 440], according to which the shear strength of a water-saturated clay-rich soil of very low hydraulic permeability, in mechanical tests of modest duration, is not altered by changing the confining pressure from its in-situ value, so that the material behaves in this respect as though it had angle of internal friction (ϕ) equal to zero.

Applicability of the $\phi = 0$ concept depends on the time scale T^* for equilibration of the pore pressure with the external water pressure by flow of water out of or into a till specimen. This is described by consolidation theory [*Lambe and Whitman*, 1969, p. 406-412]. The equilibration time scale is $T^* = H^2/c_v$, where $2H$ is the specimen thickness (through which the pore water flows) and c_v is the till's hydraulic diffusivity (called "coefficient of consolidation" by *Lambe and Whitman* [1969, p. 407]). From oedometer tests on a till specimen 22 mm thick, by fitting the observed consolidation-vs.-time curve to the theoretical curve given by *Lambe and Whitman* [1969, Figure 27.3] Hermann Engelhardt determined $c_v = 7.4\times10^{-9}$ $m^2\ s^{-1}$. For a 2-m-long core in its core tube, for which the pore water flow is along the length of the core, the time scale is thus $T^* = 1.0^2/7.4\times10^{-9} = 1.35\times10^8$ s = 4.3 years. Because the half hour needed to bring the core up from depth is only a small fraction of the equilibration time scale, only a small amount of pore-water flow will take place, and the $\phi = 0$ concept is applicable. This conclusion is linked to the till's very low hydraulic conductivity (2×10^{-9} m s^{-1} as measured by *Engelhardt et al.* [1990, p. 58]), since c_v is proportional to the conductivity.

When the recovered core reaches the surface and is removed from the core tube its pore pressure will usually be negative by a fraction of a bar because of the positive effective pressure inherited from its in-situ condition (Section 7.4). If it is then removed from the core tube and immersed in water, it will imbibe water on a time scale T^* of about a day, but if not immersed, capillary tension can maintain the negative pressure [see *Lambe and Whitman*, 1969, pp. 246, 315, 316]. This is probably why till core specimens retain a measureable shear strength in storage over times of many months (Sections 6.1, 6.2), contrary to what would be expected from the T^* limit on applicability of the $\phi = 0$ concept.

6.1 Shear Creep Tests on Freshly Sampled Till

At one location on Ice Stream B (borehole 89-1) and one on Ice Stream D (borehole 98-2) a sample of the till

* I use the term "treiboplastic" in preference to "Coulomb-plastic" because it is more self-explanatory and more compact.

recovered by coring was subjected in the field to direct shear tests [*Lambe and Whitman,* 1969, p. 119] in the creep mode, in which the sample is subjected to a constant load in simple shear and the shear strain rate is observed as a function of time, for various values of the applied shear stress. The till from Ice Stream B (core 89-1-3), behaved as follows [*Kamb,* 1991, p. 16,587]. At stresses below about 2 kPa, the till showed transient creep, decreasing with time [*Singh and Mitchell,* 1968]. Above about 2 kPa it showed accelerating creep leading promptly to catastrophic failure, the promptness of which increased drastically with attempts to apply shear loadings greater than 2 kPa. This type of behavior is what is expected for a plastic material, with an indicated shear strength of 2 ± .2 kPa. The till from Ice Stream D (core 98-2) behaved similarly, with an indicated shear strength of 1 ± .2 kPa.

6.2 Direct Shear Tests in the Laboratory

Subsequent to their return to the U.S., till samples from Ice Stream B were extensively tested in direct shear under controlled shear rate, in apparatus kindly made available by Prof. Ronald Scott in the Caltech Engineering Division. The tests were carried out by Hermann Engelhardt. The diameter of the (circular) sample chamber (shear box) was 6.35 cm, and the shear gap between the upper and lower halves of the shear box was 4.6 mm. Clasts greater than ~10 mm in size, constituting less than 2% of the test sample volume, were removed from the till before testing, because they would tend to interfere with the tests. The samples tested were from core 89-1-4. Most of the tests were on till from near the top of the core. The tests were done about 8 months after original recovery of the core.

Examples of the test results are given in Figures 10, 11, and 12. These were nominally "drained" tests at atmospheric pressure, but because of the till's extremely low hydraulic conductivity (Section 6) its water content could have changed only slightly during each run (lasting at most 2 or 3 hours, whereas $T^* \approx 1.5$ days), so that the tests were effectively "undrained". To avoid evaporative water loss during testing, the surface of the test specimen exposed to the air (in the shear gap) was kept wet by administration of drops of water. The till in these tests was under a nominal normal stress of 9 kPa due to the weight of the test specimen and an overlying thin piston (steel plate). According to the $\phi = 0$ concept, this normal stress should not affect the measured strength. The confining pressure could not be increased above this level without producing extrusion of the sample through the shear gap of the testing machine.

Figure 10 shows tests at three different shear rates spanning a 58-fold range from 0.09 to 5.2 md^{-1}. Essentially all of these tests reached a full "mobilization" of strength (i.e. reached essentially constant stress) within the 8 mm of shear displacement permitted by the testing machine. The average strengths are 1.62 ± 0.09 kPa at shear rate 0.09 md^{-1}, 1.65 ± 0.08 kPa at 0.86 md^{-1}, and 1.72 ± 0.08 kPa at 5.2 md^{-1}. Thus the strength is nearly constant at about 1.7 kPa but increases slightly with strain rate. The strength 1.7 kPa is roughly the same as the value 2 kPa obtained in Section 6.1. Thus there was not a substantial loss (or gain) of pore water and a corresponding change in strength (Section 6.5) in the 8 months between the two sets of tests.

It is customary to report the dependence of the strength on the strain rate in terms of a quantity S, the percentage variation in strength per decade variation in strain rate (see

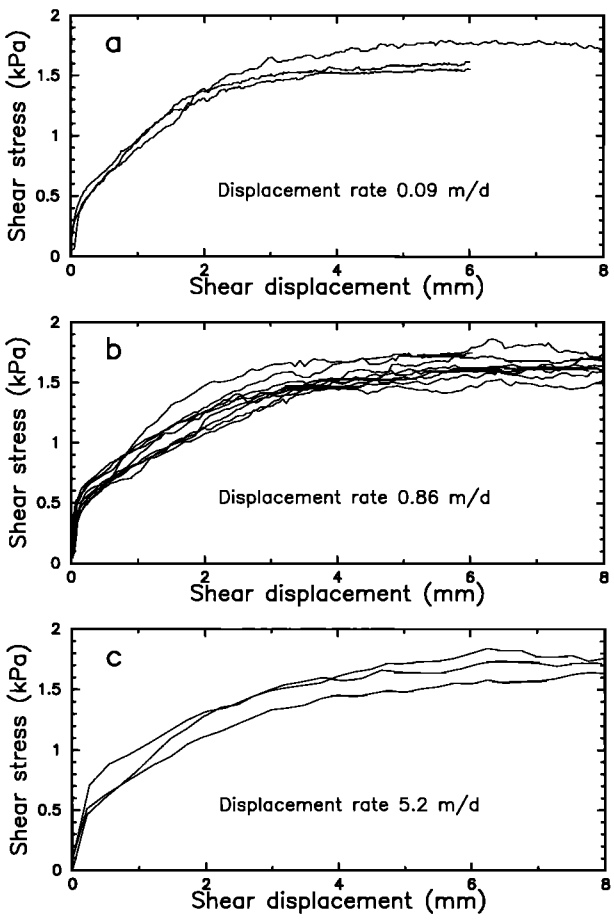

Figure 10. Direct shear tests of till from core 89-1-4, at three shear rates: (a) 0.09 m d^{-1}; (b) 0.86 m d^{-1}; (c) 5.2 m d^{-1}.

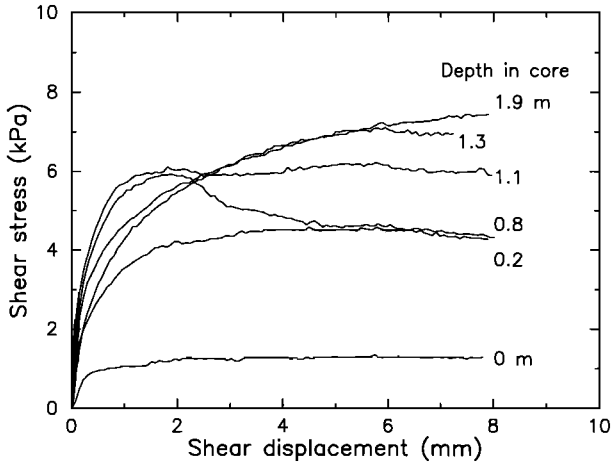

Figure 11. Direct shear tests of till samples from a succession of depths below the ice-till interface in core 89-1-4. Depths in meters as indicated. Shear displacement rate 1.25 m $d.^{-1}$

Section 6.6). In these terms, the dependence indicated by the above tests is $S = 3.4\%$ per decade. The S value is calculated from paired (shear strength, shear strain rate) data $(\tau_1, \dot{\gamma}_1)$ and $(\tau_2, \dot{\gamma}_2)$ by the relation

$$S = 100 \ln 10 \log(\tau_2/\tau_1)/\log(\dot{\gamma}_2/\dot{\gamma}_1)$$

which follows from equations (10) and (11), derived in Section 6.6.

In the 16 direct-shear tests plotted in Figure 10 there is little indication of any tendency for the strength to decrease at large strain to a "residual strength", as it does typically in tests on very clay-rich soils [*Skempton*, 1985]. A test of the till in a ring-shear device, which is capable of very large shear displacements, showed a 5% decrease in strength for a shear displacement of 200 m [*Tulaczyk et al.*, 1999a, Figure 3B]. Occasionally direct-shear tests showed a much larger decrease following a peak (e.g. one of the curves in Figure 11), but this appears to be an anomaly, caused perhaps by relatively large clasts getting caught between the edges of the shear gap and then working loose, or by overconsolidation of the till involved.

Figure 11 shows results of a series of direct-shear tests on till samples from a succession of locations down along the 89-1-4 core. The sample locations are identified in terms of their depth in meters below the top of the core. The sample at the top of the till (at depth 0 m) has a much lower strength than any of the others, which were from depths of 0.2 m or more below the top of the till. This suggests that if the till is undergoing shear deformation in situ, the shear is concentrated in or limited to a relatively thin ($\leq$ 0.1 m) shear zone at the top of the till, which agrees with the results of the basal sliding measurements on Ice Stream B (Section 5).

Figure 12 shows direct-shear test results for till specimens with a range of water-saturated porosities. They illustrate an important tenet of soil mechanics, that the strength of a water-saturated, clay-rich granular medium is a decreasing function of its porosity [*Lambe and Whitman*, 1969, p. 305]. In a general way this provides a relation between Figures 11 and 8—the increased strength of the deeper till samples being what is expected if the till porosity decreases with depth as in Figure 8b. This topic is considered in more detail in Section 6.5.

6.3 Triaxial tests

In relation to direct-shear tests, triaxial tests have the advantage that both the confining pressure and the pore water pressure can be controlled independently, in addition to the applied deviatoric stress (resulting in applied shear stress). Six sets of undrained triaxial tests, on six till samples from depth 1.5-2.5 m in core 92-1, were carried out by *Tulaczyk* [1999, Chapter 4] (see *Tulaczyk et al.* [2000a, p. 467]). Each test set began with a pressurization of the pore water to eliminate air bubbles, followed by preconsolidation at a chosen effective pressure. Deviatoric stress was then applied by axial compression, reaching specimen failure at axial strain ~2-4% and continuing to strains as large as 25%.

Results of three of the tests are plotted in the Mohr diagram in Figure 13. A Mohr circle is plotted for each test on the basis of the applied effective principal stresses

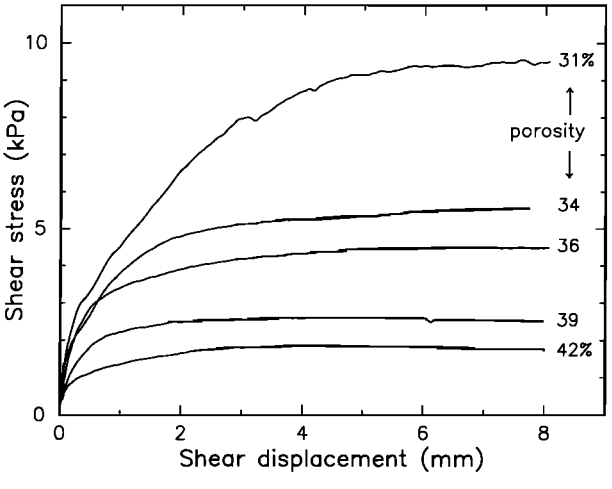

Figure 12. Direct shear tests of till with a succession of water-saturated porosities as indicated. The porosities were obtained by reconstituting dried till samples from core 89-1-4 with weighed amounts of water.

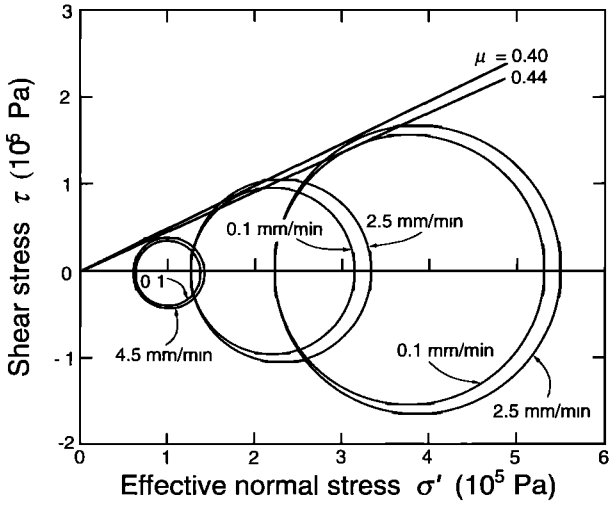

Figure 13. Mohr plot of results of three triaxial tests of till, each test at two strain rates. The strain rates are given in terms of shear displacement rates across the theoretical shear-failure plane for internal friction $\mu = 0.44$. Till is from near the top of core 92-1. Data from S. Tulaczyk (personal communication, 1999).

at failure (i.e. at full strength mobilization). The pattern of circles with common tangent lines is the pattern expected for a treiboplastic material. The indicated coefficient of internal friction is $\mu = 0.45$, the angle of internal friction $\phi = 24^\circ$, and the cohesion ~1 kPa.

Figure 14 compiles all failure stress values (shear stress and corresponding effective normal stress at failure) for all of the six sets of tests. The shear stress and effective normal stress values are those acting across the theoretical shear plane for Coulomb failure, inclined at the angle $45^\circ - \phi/2$ to the compression axis; they are calculated from the effective principal stresses at failure in each test. The results in Figure 14 are fit by the straight line with slope angle $\phi = 23.9^\circ$, slope $\mu = \tan \phi = 0.443$, and intercept (cohesion) = 1.3 kPa. In relation to the range of shear stresses over which these parameters are experimentally determined, 20 kPa $\leq \tau_f \leq$ 150 kPa, the cohesion ~ 1 kPa is essentially nil.

The triaxial tests were carried out at many different strain rates over a wide range, so as to search for a strain-rate dependence of the yield strength of the till—that is, for viscous or quasiviscous behavior. An example is Figure 13, where the larger circle of each close pair is the result for a test at higher strain rate (higher by a factor of 25 to 75). From the strain-rate ratios (see figure caption) and the ratios of the circle diameters one finds $S = 4\%$, 5%, and 6% per decade for the three pairs of tests in Figure 13. Another example is in Figure 15, which shows the axial stress recorded for a specimen shortened alternatingly at four different axial strain rates. The variations in stress are ≈ 6% for 5-fold variations in strain rate, which corresponds to $S \approx 4\%$ per decade. In Figure 16a all values of normalized shear strength, from runs generally like Figure 15, are plotted against the corresponding rates of shear strain across the theoretical shear plane, calculated from ϕ and the measured axial strain rate. The shear strength values are normalized with the preconsolidation effective pressure for each run, which suppresses the strong dependence of strength on effective pressure. The slope of the line in Figure 16a corresponds to a strain-rate dependence $S = 11\%$ per decade at $\dot{\gamma} = 2 \times 10^3\ a^{-1}$.

6.4 In-situ Strength of Till

The primary interest is in the strength of the till in place, under the ice streams. As noted in Section 6, the $\phi = 0$ concept and the effects of negative pore pressure in principle permits the in-situ strength to be measured from till cores if the measurement is made soon enough after the core is taken. "Soon enough" is a somewhat vague requirement, although the reasoning in Section 6 and the data in Sections 6.1 and 6.2 suggest that the shear strength of till samples stored in sealed containers does not change much over time scales of a few days to 8 months. The triaxial tests do not directly indicate in-situ strength because of the preliminary steps of pore pressurization and preconsolidation (Section 6.3). They could provide an indirect indication from the Coulomb failure condition if the in-situ effective pressure were known, but this quantity is uncertain (see Section 7). To get around these

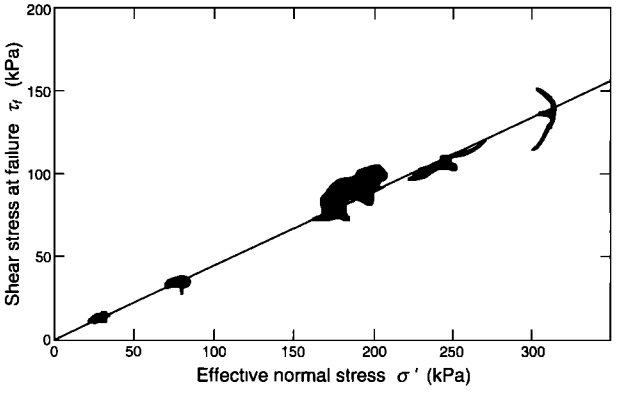

Figure 14. Triaxial test data from six sets of undrained tests on till from core 92-1 [*Tulaczyk et al.*, 2000a, Figure 5A]. Abscissa is effective normal stress across the calculated theoretical shear failure plane. The individual data points (numbering 3264) from the original work are not shown; instead, the distribution of data points is shown by dark shading.

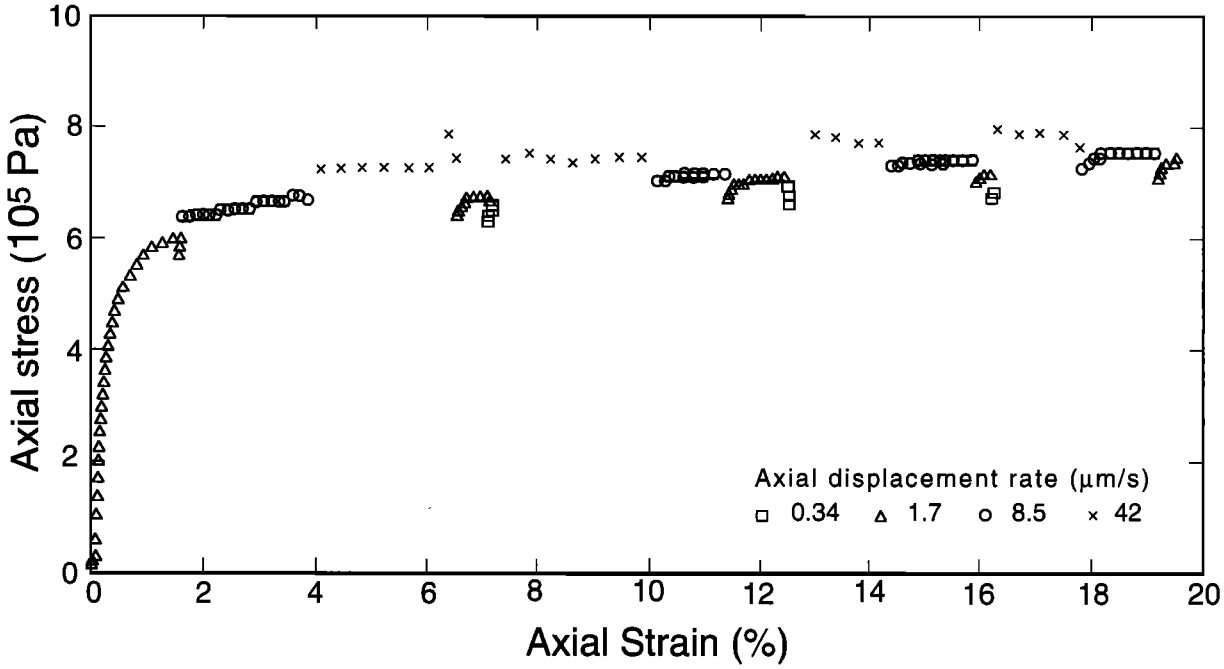

Figure 15. Triaxial test of till sample with alternation among four strain rates, as indicated at lower right. Axial strain rate is given in terms of the axial displacement rate in μms^{-1}. The test specimen is from core 92-1. Original specimen length was 6.5 cm. Data from S. Tulaczyk (personal communication, 1999).

difficulties we have developed and used a torque-vane instrument ("torvane") to measure the in-situ till strength directly. It is a version of an instrument used in soil mechanics [*Lambe and Whitman,* 1969, pp. 79, 451]. The torvane, which is pictured in Figure 5, measures the torque required to rotate a four-bladed (cross-shaped) vane that has been pushed down into the till at the bottom of a borehole. The rotation rate, and hence the strain rate of the till, can be varied over a 64-fold range.

Calibration of the instrument response (kPa of shear strength per volt of instrument output) was done by measuring a water-saturated test soil ("McMurdo silt") with the borehole torvane and with a commercially made and calibrated "hand vane tester" (EDECo "Pilcon" DR 3749). Calibration can also be done by measuring the torque/output-voltage response of the instrument and relating it to strength by a simple theoretical assumption as to the shear stress distribution around the rotating vane. This second calibration method gives a response factor (kPa V^{-1}) about twice as large as the first method, so the calibration has to be considered uncertain to this rather large extent. We report our results here in terms of the first method of calibration (which gives a response factor of 5 ± 1 kPa V^{-1}).

Results for borehole 91-1 at Up B are in Table 4. The indicated average shear strength of the basal till is about 2 kPa. Dependence of strength on shear strain rate is on average nil ($S = 0\%$ per decade) over 16- to 64-fold ranges in strain rate. These features confirm that the results of the direct-shear tests on till core material (Sections 6.1, 6.2) are applicable to in-situ conditions, and thus that reliance on the $\phi = 0$ concept is valid. The strength data in Table 4 and similar data from New B (borehole 95-1) and Up C (holes 96-4 and 96-6) are summarized in Table 5. They indicate that the in-situ till strength at New B is somewhat greater than at Up B, and is about 2.5 times greater at Up C. The strength of 1.0 ± 0.3 kPa for Up D in Table 5 is not from the torvane (which suffered an electrical malfunction) but from direct shear tests carried out on till from core 98-2 immediately upon core recovery (Section 6.1).

The till strength under Ice Stream C may be larger than the value measured with the torvane because of possible disturbance of the till by the hot-water jet once breakthrough has occurred (Section 7.1). The jet doubtless mixes some water into the upper part of the till, which weakens it (Section 6.5). The jet must also winnow the till and produce sorting and grading in a resedimentation process, much as it does in boreholes that bottom in frozen till (Section 4.5). These disturbances must affect the Ice-Stream-B till also, but the rapid basal sliding (Section 5) presumably displaces the disturbed area away from the bottom of the borehole by the time the torvane or piston

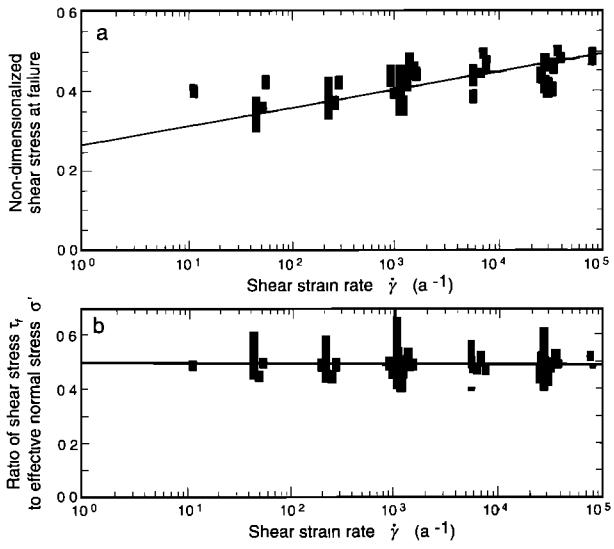

Figure 16. Triaxial test data showing dependence of till shear strength on strain rate. (a) Yield stresses from the data base for Figure 14 are here normalized by the preconsolidation pressure for each test series (such as Figure 15), which suppresses the strong dependence of strength on the general level of effective stress in the tests without bringing into consideration any variation of pore pressure or effective stress with strain rate. Shear strain-rates across the theoretical failure plane are as calculated from the measured axial strain rates. As in Figure 14, only the distribution of data points is shown, not the individual points. (b) Yield stresses from the data base for Figure 14 are here normalized by the effective normal stress in each test (each cluster of data points in Figure 15), which brings in the effect of the measured pore pressure on the effective stress in each test. Because the yield stresses normalized in this way show no dependence on strain rate, the dependence seen in (a) is demonstrated to be the result of a dependence of pore pressure on strain rate. Data from *Tulaczyk et al.* [2000a, Figures 5B and 5C].

corer reaches it. Such replacement of disturbed till by undisturbed till should not occur in Ice Stream C, because it presumably has little basal sliding, its streaming flow having nearly stopped. Most of the piston cores from Ice Stream C appear to be normal till, undisturbed by winnowing or resedimentation but core 96-6 gave an x-ray image that seems to show fining- upward grading in the uppermost 0.2 m of the core. Also, three of the Ice Stream C cores contained a sorted sand layer ~1 cm thick at the top of the core (S. Tulaczyk, personal communication, 1999). These facts suggest that some winnowing of till sediment by the hot-water drill is recorded in these cores.

There might be concern that the drilling of the borehole in which a torvane measurement is made has relieved the ice overburden stress and therefore the effective pressure, resulting in a falsely weak shear strength, so that the true in-situ strength is not measured. There are three reasons why this is not a concern: 1. When the ice is melted in drilling the borehole the ice overburden stress is replaced by the basal water pressure, which is nearly the same (Sections 3.2 and 7.4). 2. Any relief (or augmentation) of the confining pressure because of this replacement presumably acts over the cross-sectional area of the bottom of the borehole, some 10 cm in diameter, while the torvane is placed at a depth of ~50 cm in the till (Table 4), where the stress relief (or augmentation) is attenuated by redistribution of the unloading (or loading) through the surrounding till, with an attenuation factor probably of the order $(10/50)^2$. 3. Because of the low hydraulic conductivity of the till, the effective pressure will initially react to the change in loading as though undrained, and will then adjust by pore-fluid flow on a time scale $T^* \sim H^2/c_v$ (Section 6) where H is the depth of the torvane in the till, so $T^* \sim 1$ year; this is so much longer than the time-scale of the torvane measurement (a few hours) that the strength measured will differ inappreciably from the in-situ strength.

In the above torvane tests, adhesion of till to the torvane (Figure 6) indicated that the instrument penetrated the till to the depths indicated in the last column of Table 5. The recorded strengths were measured with the vane at these depths. (In the case of Ice Stream D the depth given is the depth in the core from which the tested sample was taken.) These data do not suggest a dependence of strength on depth in the till. In several tests in Ice Streams B and C an effort was made to measure with the torvane a profile of strength up through the till. An example of such a profile from Ice Stream C is given in Figure 17. These results, though somewhat problematical, seem to indicate that the

Table 4. In-situ Strength of Till Measured with Torvane in Hole 91-1 as a Function of Shear Strain rate $\dot{\gamma}$ (represented by vane rotation rate)

	Till strength		Vane rotation rate	
Test No.	at low $\dot{\gamma}$ (kPa)	at high $\dot{\gamma}$ (kPa)	at low $\dot{\gamma}$ (r.p.hr.)	at high $\dot{\gamma}$ (r.p.hr.)
1	2.0 ± 1.5	2.1 ± .5	1	16
2	1.5 ± .1	1.4 ± .1	1	16
3	2.3 ± .05	2.1 ± .05	0.5	32
	-	1.9 ± .05	-	32
4	2.1 ± 1.0	2.3 ± .2	0.5	32
	-	2.1 ± .1	-	32
(av)	2.0 ± 0.3	2.0 ± 0.3	~1	~30

Table 5. In-situ Till Strength: Summary

Study site	Borehole	No. of tests	Strength (kPa)	Depth in till (cm)
Up B	91-1	4	2.0 ± .3	59, 66
New B	95-1	7	2.7 ± .5	35
Up C	96-4	7	3.9 ± 1.0	15 - 20
"	96-6	2	5.5 ± .3	70
"	"	20	4.5 ± 1.0	70
Up D	98-2	10	1.0 ± .3*	42

* Direct shear tests on core sample just after core recovery

strength drops by ~50% in the uppermost 0.5 m of the till, suggesting a shear zone at the top of the till.

6.5 Dependence of Strength on Water Content of Till

Triaxial test results shown in Figure 18 verify for the till the empirical relationships found in soil mechanics between pore volume and effective pressure under loading that compresses or consolidates (compacts) the soil, or under unloading, which allows the soil to expand. The empirical relations, shown by the lines in the figure, are described by *Clarke* [1987, p. 9026]. They are linear relations between the logarithm of the effective pressure σ' (total confining pressure minus pore water pressure) and the void ratio $e = V_w/V_s$ where V_w is the water-saturated pore volume in a given mass of till and V_s is the total solid-particle volume in the same mass. The "Normal Consolidation Line" (NCL) is the e-vs.-σ' path followed under increasing effective pressure applied to a "virgin" till sample that has not been previously consolidated under an effective pressure as high as that being currently applied, or whose "virginity" has been restored by reworking ("remolding") under low effective stress. The empirical NCL relationship is

$$e = e_c - C_c \log(\sigma'/\sigma_c) \qquad (1)$$

where σ_c is a reference effective pressure, e_c a reference void ratio, and C_c a constant called the compression index. In Figure 18 the heavy line labeled "NCL(ISO)" represents (1) for isotropic consolidation, which can be effected in the triaxial apparatus, while the dashed line labeled "NCL (UNI)" is for consolidation that is confined laterally so that the lateral strains are zero (uniaxial compression). The latter is the consolidation geometry provided by standard "oedometer" consolidation-testing machines. The fine broken line labeled "URL (5.7)" ("unloading and reloading line") is an example of the e vs. σ' path followed upon unloading from a point on the NCL (in this case the point at $\sigma' = 5.7$ bar) and also upon reloading up to that point.

In Figure 18 the fine continuous line labeled CSL, the "Critical State Line", is the locus of (σ', e) states that are attained under shear deformation superimposed upon consolidation, which is the condition of most interest here. The CSL and URL are empirical relations analogous to (1); for example, for the CSL,

$$e = e_f - C_f \log(\sigma'/\sigma_f) \qquad (2)$$

The subscript "f" here refers to the condition of shear failure. The NCL(ISO) and CSL for the till were determined by *Tulaczyk* [1999, Chapter 4] by least-squares fit to triaxial test data (e.g. the data for the NCL (ISO) in Figure 18), while the NCL(UNI) and URL are from oedometer data obtained by Hermann Engelhardt. Numerical formulation of these lines is given in Figure 18. Note that $C_f = C_c$, as is generally expected.

Equation (2) provides the basis for a quantitative relation between till strength and water content (expressed as void ratio e). If the strength τ_f is assumed to obey the Coulomb failure condition with negligible cohesion:

$$\tau_f = \mu\sigma' \qquad (3)$$

then combining (2) and (3) and rearranging gives

$$\tau_f = \mu\sigma_f \exp[(e_f - e)\ (\ln 10)/C_f] \qquad (4)$$

This is an inverse relation between shear strength τ_f and void ratio e or porosity $\pi = e/(1+e)$. It plays an important role in Tulaczyk's new theory of ice stream mechanics (Section 9.2).

The inverse relation (4), in qualitative terms, was noted in Sections 6.2 and 6.4 and an example was shown in Figure 12. When this example is evaluated according to (4), the indicated value of the constant C_f is 0.38, quite different from the $C_f = 0.12$ found by the triaxial tests (see formula for CSL in Figure 18). The reason for the discrepancy is not known but may have to do with the fact that in the tests in Figure 12 the pore water pressure could

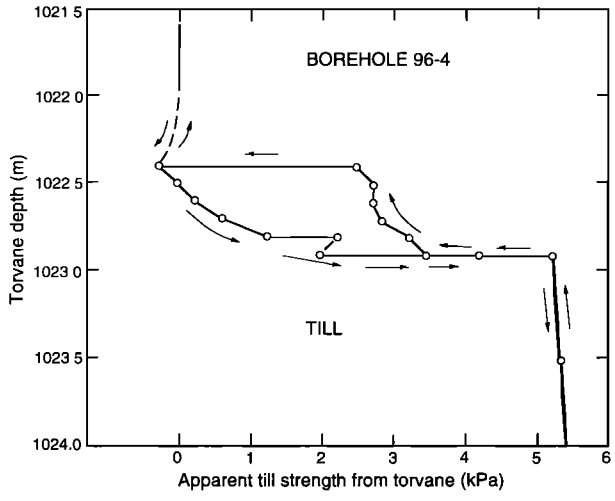

Figure 17. Vertical profile of till strength measured with the torvane in borehole 96-4. The top of the till is at nominal depth 1022.4 m. Arrows indicate the measurement sequence.

not be directly controlled. If we calculate from (4) the till strength that corresponds to the observed till porosities, we obtain a rather large scatter of values. They are shown in Table 6, for porosity ranges and averages found in Ice Streams B, C, and D (Table 3), and for the two versions of equation (4) based on Figures 18 and 12 as discussed above. The latter version gives strength values that seem more reasonable in relation to the till strengths determined by other means (Sections 6.1, 6.2, 6.3, and 6.4).

The inference of basal-till shear strength from till porosity is discussed more fully in a paper by *Tulaczyk et al.* [unpublished]. It concludes that basal effective stresses σ' as low as 2 kPa can be inferred from the data. This is much smaller than the average values 20-60 kPa that would seem to be indicated by the directly measured basal pressures (Section 3.2). From the low inferred value $\sigma' \sim$ 2 kPa, a basal shear strength as low as about 1 kPa is indicated, in general agreement with direct shear measurements on till specimens from near the base of the ice (Sections 6.1 and 6.2).

6.6 Rheological assessment

The results of the mechanical tests on the till in Sections 6.1-6.5 conform fairly well to the attributes of treiboplasticity: a failure strength that is a linearly increasing function of the effective normal stress, that is independent of the strain rate, and that depends on the water-saturated porosity according to a relation that is linear in a semi-log plot. Treiboplasticity therefore seems to provide a good first approximation to the till's mechanical properties. Its internal friction is 0.44 and its apparent cohesion is ~ 1 kPa, values that are typical of soils with ~35% clay content [*Kedzi,* 1974, Table 28; *Terzaghi et al.*, 1996, Fig 19.7; *Lambe and Whitman,* 1969, pp. 307, 313].

In a second approximation the till strength depends slightly on the strain rate. This has significant consequences in the formulation of a rheology for the till. If the till behaves as a perfect treiboplastic material, with strength fully independent of strain rate, its deformation represents a rheologically singular situation in which, as in the perfect plasticity of metals [*Hill,* 1950] and perfectly plastic ice [*Nye,* 1951], the flow is not fully controlled by the stresses and a flow law of conventional type (strain rate as a completely determined function of stress) cannot be written. If however there is an appreciable strain-rate dependence of the strength, the treiboplastic failure condition can be reformulated as a flow law, and the flow mechanics assumes a more familiar form, one that may be more advantageous for numerical modeling than is the perfect-treiboplasticity formulation. It is therefore of practical as well as fundamental interest to consider how much the till rheology deviates from perfect treiboplasticity and to compare it in these terms with the rheology that has been used in ice-stream modeling.

This can be done with a measure of the strain-rate dependence of the strength. As noted in Section 6.2, it is standard practice to take as a measure of this dependence the percentage variation in strength per decade of variation in strain rate, a quantity here designated S. The values of

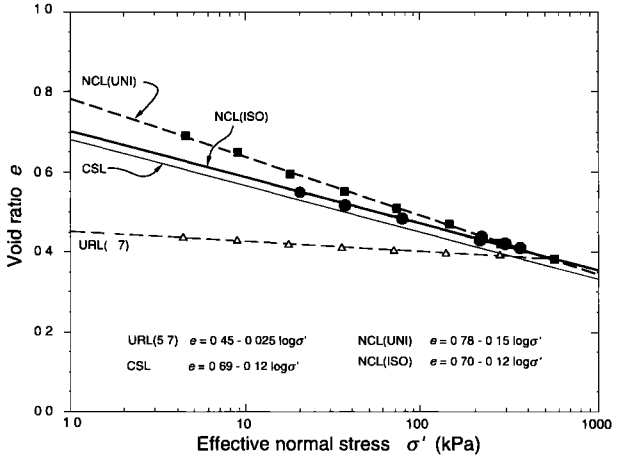

Figure 18. Data from consolidation tests on till. The data for the isotropic NCL and the CSL are from triaxial tests by S. Tulaczyk, and the data for the uniaxial NCL and the URL (for preconsolidation pressure 5.7 bar) are from oedometer tests by H. Engelhardt. See *Tulaczyk et al.*, [2000a, Figure 6A].

Table 6. Calculated Till Shear Strength (kPa) from Equation (4) for Observed Ranges of Porosity (low, average, high) and two Values of the Compression Index C_f

Ice Stream	Porosity π (%)	Calc. 1 τ_f (kPa)	Calc.2 τ_f (kPa)
B	36	5.1	7.9
"	40	0.7	2.3
"	46	0.02	1.0
C	33	19.5	6.8
"	42	0.2	1.6
"	51	5×10^{-4}	0.2
D	44	0.07	1.0
"	48	0.01	0.5
"	53	10^{-4}	0.1

Calculation 1: $C_f = 0.12$, from Figure 18
Calculation 2: $C_f = 0.38$, from Figure 12

S reported in Sections 6.2, 6.3, and 6.4 from the various sets of tests are 3.4, 4, 5, 6, 4, 11, and 0% per decade (on average $S = 5\% \pm 3\%$ per decade). S values of this order are commonly encountered for soils and fault gouges as reported in the literature [*Berre and Bjerrum*, 1973, p. 6; *Bishop et al.*, 1971, p. 302; *Blanpied et al.*, 1987, Figure 3; *Marone et al.*, 1990, Table 2; *Sheahan et al.*, 1996, Table 1; *Skempton*, 1985, p. 14; *Kamb* 1991, p. 16,586; *Scholtz*, 1998, Figure 1A].

As is shown below, an S-type dependence of strength τ_f on strain rate $\dot{\gamma}$, in which S is constant, independent of τ_f or $\dot{\gamma}$, can be expressed as a nonlinear flow law of the standard form $\dot{\gamma}/\dot{\gamma}_o=(\tau_f/\tau_o)^n$, where $\dot{\gamma}_o$, τ_o, and n are constants, and the exponent n is related to S by $n = (100 \ln 10)/S$. From this relation, the n values that correspond to the S values given above range from 21 to ∞ and cluster around 40. This represents a nonlinearity that is extremely large in relation to typical nonlinearly quasiviscous materials, which generally have $n \lesssim 5$ [*Garofalo*, 1965, p. 50]. The nonlinearity is so large that the till can be considered to behave rheologically much more nearly as a perfect treiboplastic material (for which $n \to \infty$) than as a normal nonlinear fluid. However, in view of the strain-rate dependence ($S \neq 0$), which is not an attribute of perfect treiboplasticity, we should use some qualified designation like "imperfect treiboplasticity" in referring to the till rheology.

The conclusion that the till rheology is essentially (though imperfectly) treiboplastic is consistent with in-situ till strength measurements in a Swedish glacier [*Hooke et al.*, 1997] and laboratory ring-shear tests on two northern hemisphere tills [*Iverson et al.*, 1998]. The latter tills differ from ice-stream till in having a strength that decreases slightly with strain rate ($S \approx -3.5\%$ per decade, $n \approx -60$). Negative S is sometimes encountered in soil mechanics [*Lambe and Whitman*, 1969, p. 314], and also in fault-gouge mechanics [*Blanpied et al.*, 1987, Figure 3; *Scholtz*, 1998, Figure 1A] where it is called velocity weakening.

In great contrast with $n \sim 40$ (or $n \approx -60$) is the near linearity ($n = 1.33$) of the quasiviscous till flow law put forward by *Boulton and Hindmarsh* [1987, equation 2, p. 9063] on the basis of measurements in a basal tunnel at the terminus of an Icelandic glacier. Reservations about the data interpretation that leads to the value $n = 1.33$ have been expressed by *Iverson et al.* [1997, p. 1058], *Hooke et al.*[1997, p. 173)] and *Iverson et al.* [1998, p. 635].

In formulating a second-approximation till rheology it is important to try to ascertain the cause and significance of the small but non-zero S values. This is a somewhat obscure subject, little discussed in soil-mechanics texts. Some clarity is provided by separately considering tests made under drained conditions, such as the ring-shear tests of *Iverson et al.* [1998], and those made under undrained conditions, such as the triaxial tests in Section 6.3. For undrained tests *Lambe and Whitman* [1969, p. 445] make the following observation: "In all cases where it has been possible to measure the pore pressures during undrained tests at various rates of loading, it has been found that the change in undrained strength results from a difference in induced pore pressure [*Richardson and Whitman*, 1964]. Increasing the rate of strain [causes reductions in] induced pore pressures." A reduction in pore pressure results in increased effective pressure and therefore increased strength. The above observation is confirmed by the triaxial test data for the till: In Figure 16b the ratio of shear strength to effective normal stress for each data point in Figure 14 (see figure caption) is plotted as a function of the corresponding applied strain rate. The result, which includes the effect of the measured pore pressures via their contribution to the effective normal stress value for each data point, shows that the ratio, and hence the strength at a given effective normal stress, does not depend on strain rate. Thus the increase of strength with strain rate shown in Figure 16a is explained as a mechanical effect of reduction in pore pressure induced by increase in strain

rate. There is no need for viscous flow elements in the system, although such elements are occasionally alluded to in soil mechanics [e.g. *Lambe and Whitman,* 1969, p. 314; *Mitchell,* 1993, pp. 318, 340].

To use the above conclusion in formulating till rheology, an explanation is needed for the strain-rate induced reduction in pore pressure. It may be attributed to an effect of strain rate on the critical-state porosity (Section 6.5): the CSL in Figure 18 is shifted upward in response to increased strain rate. The consequent tendency for the till to dilate when its strain rate increases has to be counteracted by a reduction in pore pressure so as to maintain a constant pore volume as required by the undrained character of the tests.

Remaining unexplained is the cause of the assumed effect of strain rate on the CSL. Also unexplained is why the S value is so variable from one test to another, and why the internal friction indicated by the ordinate of the horizontal line in Figure 16b is 0.50 rather than 0.44 or 0.45 as determined in Section 6.3.

Iverson et al. [1998, p. 638], following *Tika et al.* [1996], offer the following explanation for the negative S value found in their tests. Because ring-shear tests are inherently drained (if conducted slowly enough for equilibration of pore pressure), the pore pressure is fixed and does not play a role in the response to strain rate. Other factors can therefore make their effect felt. In particular, if increased strain rate raises the CSL, as suggested in the previous paragraph, the deforming till will dilate to follow it. This will result in a less dense framework structure with lessened particle interlocking and with consequent decrease in the angle of internal friction ϕ and therefore in the strength at given effective pressure. Again, a mechanism for coupling the strain rate to the CSL is needed.

It would seem that Iverson et al's. explanation should apply to the direct shear tests in Section 6.2, whereas the tests actually showed variably positive S. Because of the very low hydraulic permeability of the till, it is likely that the pore pressure did not have time to equilibrate fully during the tests, so that the tests had some undrained character and some of the pore-pressure effect resulting in positive S was felt.

"Probably the exact nature of the strain rate effect varies from soil to soil" [*Lambe and Whitman,* 1969, p. 314].

Based on the above discussion of strain-rate dependence of strength there are two ways to proceed in trying to formulate a second-approximation rheology for the till: I. Rheology based on mechanism(s) of strain-rate dependence. II. Rheology on a purely empirical basis. In method I, known or assumed dependences on $\dot{\gamma}$, such as the CSL and ϕ dependences discussed above, are introduced into the standard Coulomb failure condition (3) (with cohesion = 0). This is illustrated as follows for the undrained situation described above. Represent the effect of $\dot{\gamma}$ on the CSL by its linearized effect on the ordinate intercept in (2):

$$e=(e_f + g\dot{\gamma})-C_f \log(\sigma'/\sigma_f) \tag{5}$$

in which the coefficient g (unrelated to gravity) is

$$g=\left\langle de_f/d\dot{\gamma}\right\rangle \tag{6}$$

Here $\langle\ \rangle$ represents an averaging from $\dot{\gamma}=0$ to the current value of $\dot{\gamma}$. For undrained conditions, hold e constant at the value e_o (value of e for $\dot{\gamma}=0$) and solve (5) with (3) to get τ_f in the same way as (2) was solved with (3) to get (4):

$$\tau_f = \mu\sigma_f \exp[(\ln 10)(e_f - e_o + g\dot{\gamma})/C_f] \tag{7}$$

Inverting for $\dot{\gamma}$ and introducing (2) with $e=e_o$ and $\sigma'=\sigma'_o$ (the value of σ' applied at $\dot{\gamma}=0$) gives

$$\dot{\gamma}=\frac{C_f}{g}\log\left(\frac{\tau_f}{\mu\sigma'_o}\right) \tag{8}$$

For g positive, τ_f is seen from (7) or (8) to be an increasing function of $\dot{\gamma}$. Equation (8) has the form of a rheological flow law for the undrained till. Likewise, a flow law for the till under drained conditions could be obtained by similarly introducing also a dependence of μ on $\dot{\gamma}$ via e.

In method II one couples with the Coulomb law (3) the best established empirical relation for $\dot{\gamma}$ dependence. The obvious choice is the S-type dependence of τ_f on $\dot{\gamma}$, which is found to fit the test data generally. The S dependence is best expressed in differential form:

$$\mathrm{d}\ \ln\ \tau_f\ /\ \mathrm{d}\ \log\ \dot{\gamma}\ =\ S/100 \tag{9}$$

where log means $\log_{10}$. From (9) it follows by integration at constant S that

$$\tau_f/\tau_o\ =\ (\dot{\gamma}/\dot{\gamma}_o)^s \tag{10}$$

where

$$s\ =\ S(100\ \ln\ 10)^{-1} \tag{11}$$

Here $\tau_o/\dot{\gamma}_o^n$ represents the integration constant. The *S*-type law (10) is coupled with the Coulomb failure law (3) by recognizing that τ_o in (10) represents the values of τ_f given by (3) as a function of σ' when $\dot{\gamma} = \dot{\gamma}_o$:

$$\tau_o = \mu\sigma' \tag{12}$$

The result (10) is the inverse of the standard nonlinear quasiviscous flow law

$$\dot{\gamma}/\dot{\gamma}_o = (\tau_f/\tau_o)^n \tag{13}$$

where

$$n = s^{-1} = (100 \ln 10)\, S^{-1} \tag{14}$$

Hence in the *S*-based empirical approach to till rheology a power-type flow law (13) emerges, with a very large value of *n*, corresponding to small *s* or *S* in (14) ($S \sim 5 \pm 3\%$ per decade, and $n \sim 40 \pm 20$).

Comparing method II's (13) with method I's (8), the latter's logarithmic form represents a weak dependence of $\dot{\gamma}$ on τ_f, contrary to the expected strong $\dot{\gamma}$-on-τ_f dependence that is seen in (13) with large *n* and that corresponds to the expected weak dependence of τ_f on $\dot{\gamma}$ represented by (10) with small *s*. (The foregoing statement re (8) holds in a general way even though the "local *n* value" $n = \mathrm{d}\ln\dot{\gamma} / \mathrm{d}\ln\tau_f = (\ln(\tau_f/\mu\sigma_o'))^{-1}$ becomes very large as $\tau_f \to \mu\sigma_o'$.) This suggests that the method-I approach used in deriving (8) is somehow flawed. At the present stage of understanding of these matters it therefore seems best in formulating the till rheology to pass over the internal till mechanics that generates the strain-rate dependence of the strength and proceed directly to its empirical representation in terms of *S*, or some other parameterization if anything better can be found.

Note that (13) can be valid as a steady-state flow law only above a certain lower-limit shear stress and corresponding strain rate, below which the flow becomes transient-decreasing in accordance with the Singh-Mitchell creep equation [*Singh and Mitchell*, 1968; *Kamb*, 1991, p. 16,586]. However, this can probably be overlooked in ice-stream modeling.

The full form of the *S*-based flow law is obtained by combining (12) and (13):

$$\dot{\gamma} = \dot{\gamma}_o \left(\frac{\tau_f}{\mu\sigma'} \right)^n \tag{15}$$

with $n \sim 40 \pm 20$). It differs greatly from normal quasiviscous flow laws (e.g. for ice) not only in the very large value of *n* but also in the occurrence of $(\mu\sigma')^n$ in the denominator. The latter feature or something like it (usually $(\sigma')^m$ in the denominator with $m \neq n$) occurs in many proposed basal sliding laws [e.g. *Bentley*, 1987, p. 8855]. It also occurs in the till flow laws of *Boulton* and *Hindmarsh* [1987, p. 9063] but with values of *m* that are very low (1.25, 1.80) though not greatly different from the assigned *n* values (1.33, 0.625). .

The "Bingham fluid model" of *Boulton and Hindmarsh* [1987, equation 1, p. 9063] has a flow law further modified from (15) by replacing τ_f^n in (15) with $(\tau_f - \tau_o)^n$ for $\tau_f \geq \tau_o$, with $n = 0.625$ (sublinear!), and with $\dot{\gamma} = 0$ for $\tau_f < \tau_o$. It has been shown that this flow law is not compatible with the triaxial test data [*Tulaczyk, et al.*, 2000a, Figure 5A; *Tulaczyk*, 1999, p. 4-12]. However, a law of this type, but with much larger values of *n* and *m*, would seem to be a possible candidate alternative to (15) for representing the till's imperfect treiboplasticity. With $m = n$ it would be essentially the same as the viscoplastic flow law for landslides as formulated by *Iverson* [1985, p. 152], except that in the latter the effect of pore pressure is not included.

A variant on formulation (10) is to express the strain-rate dependence of the strength in the form

$$\tau_f/\tau_o = 1 + s \ln(\dot{\gamma}/\dot{\gamma}_o) \tag{16}$$

[e.g. *Iverson et al.*, 1998, equation 1; *Kamb*, 1991, equation 5; *Scholtz*, 1998, equation 3]. A line of this form is fitted to the strength data in Figure 16a. For small values of $s \ln(\dot{\gamma}/\dot{\gamma}_o)$, (16) and (10) are essentially the same, but for a wide range of strain rates (16) becomes only an approximation to (10). The choice between the two is purely empirical, except that the inverse of (16) expresses $\dot{\gamma}$ as an exponential function of τ_f, which has been given some justification from rate process theory (Mitchell, 1993, p. 352).

7. BASAL WATER SYSTEM

It seems reasonable to assume that water generated under ice streams by basal melting may accumulate in the basal zone or may be transported downstream in this zone, to be released into the sea at or near the (un)grounding line. The system of conduits in which such water storage and transport occurs is called the basal water system or basal

hydraulic system. It may bear some resemblance to the basal water systems of temperate glaciers, and has been treated theoretically on this basis [*Weertman and Birchfield,* 1982; *Bindschadler,* 1983, p. 10] or modifications thereof [*Alley*, 1989a]. Here the effort is to bring together the lines of observational evidence bearing on the basal water system of ice streams. Relevant hydraulic observations from Ice Stream B have been discussed extensively by *Engelhardt and Kamb* [1997] (here called "E & K"), and we can limit the treatment here to an update of that discussion. Subsequent to the observations discussed in E & K, additional observations have come from 13 boreholes drilled to the bottom of Ice Stream C and 5 holes drilled to the bottom of Ice Stream D.

7.1 System Existence and Gap Models

In the drilling of a borehole in an ice stream the existence of a basal water system is made seemingly obvious by the rapid disappearance of large quantities of borehole water down the hole starting at the moment when the drill breaks through the basal ice into the till. This has been experienced in all boreholes that reached the base in Ice Streams B, C, and D, with possible exception of holes 95-3 and 96-3 (see below) and also hole 88-2 (Section 7.7). The downrush of water is seen in terms of the rapid drop in borehole water level, typified by the quasi-exponential water-level drop curves (E & K, Figure 3). The water-level drop time ("WLDT", the time for ca. 90% of the total drop) and T, the time constant for a quasi-exponential drop curve, are generally in the range 1-3 minutes in Ice Stream B (see Table 1, last two columns). If the basal water system consists of a partially continuous gap between the bottom of the ice and the top of the till ("gap-conduit model"), then a treatment of the breakthrough drop curve by the method of *Weertman* [1970] indicates that the observed values of T correspond to a basal gap 1.4 to 2.5 mm thick (E & K, Section 9a).

The breakthrough behavior of boreholes in Ice Streams C and D is in a general way similar to that in Ice Stream B, suggesting the presence of a similar basal water system, but with a few differences as discussed below.

The first problem in interpreting the basal water system with the gap-conduit model is that the existence of the gap in the natural state, unmodified by borehole drilling, has been in question for various reasons (E & K, Sections 6, 9b, and 9d; *Tulaczyk*, 1999, Section 5.5.2). One reason is the lack of evidence that more water has ever been produced (pumped out) from the basal system than has been injected into it from the boreholes on breakthrough (E & K, Section 6). Another reason is the low measured propagation speed of the pressure pulse introduced into the till-ice interface when the drill breaks through (E & K, Section 8). This observation is best explained if in the natural state (unmodified by hot-water drilling) there is no continuous macroscopic ($\geq$1 mm) water-filled gap between ice and till, and if in the breakthrough process a gap $\geq$1 mm thick is formed by injection of pressurized water along the till-ice interface. An analysis of such a "gap-opening model" seems to indicate that it is able to account for the slow speed of pressure-pulse propagation (E & K, Section 9c). If this is so, then the gap-conduit model of the basal water system, with a ~ 2 mm natural till-ice gap that pre-exists any gap produced by borehole drilling, is ruled out.

Two new observations change this picture. First, two pressure pulse propagation experiments carried out on Ice Stream C with boreholes 96-4, 96-8, and 96-13 gave a propagation speed much faster than was found in Ice Stream B. The data (in a format like E & K, Figure 19) show a roughly instantaneous propagation, or when scrutinized more closely a propagation speed of about 2.5 m s^{-1}, about 14 times faster that the 0.18 m s^{-1} observed in Ice Stream B (E & K, Section 8). The time resolution of 5 seconds for the pressure data in these figures admits the possibility that the propagation time is essentially 0. To the extent that the pulse propagation speed approaches the speed of sound in water (1400 m s^{-1}), the data permit a pre-existing basal water system with conduits $\geq$1 mm in width or diameter, although the matter is somewhat complicated (E & K, Section 9b). In any case, the large difference between the propagation speeds at the study sites on Ice Streams B and C indicates either a major difference in the nature of a basal water system at the two sites or else the operation of unknown complicating factors at one or the other of the sites. A great peculiarity in the data from Ice Stream C is that in experiment 2, the pulse that arrived at the expected time at borehole 96-4, 50 meters from the source of the pressure pulse (hole 96-13), was a pulse of decreased rather than increased pressure (i.e., a rarefaction).

The second and the most compelling new observation was made in Ice Stream D and is shown in Figure 19. In drilling the first borehole of the season (98-1), before any disturbance of the basal system by connection to a borehole had occurred, the water level in the borehole was pumped down and became constant (with pump running) at a depth of 120 m below the surface. When breakthrough occurred, the borehole water level did not fall as usual, but instead *rose*, to a depth of 107 m. The rise time was 3 minutes. After a few minutes' wait, the pump-out pump was turned off and water was pumped into the hole. The water level

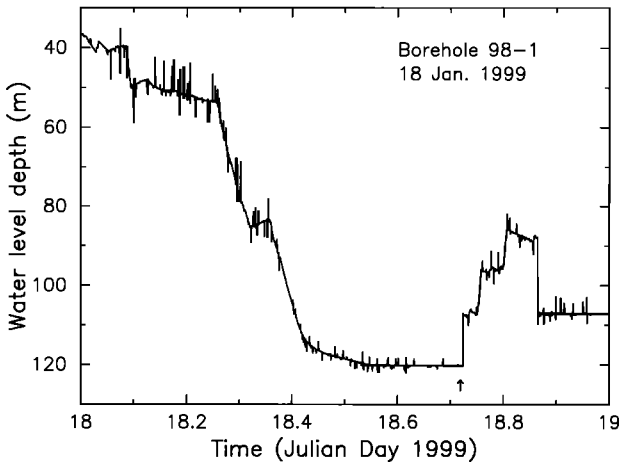

Figure 19. Rise in borehole water level on breakthrough to basal water system in borehole 98-1, Ice Stream D. The rise occurs at J.D. 18.72, marked with an arrow. The gradual drop in water level from depth 37 m at J.D. 18.0 to 120 m at J.D. 18.54 was caused by purposely pumping water out of the hole while drilling proceeded. See text for details.

proceeded to rise, and rose to 97 m depth before the pumping-in was stopped. This rise in water level showed that hydraulic connection with the basal system had been lost, probably by basal till being carried up into the borehole by the inrush of water from below. After a brief wait more water was pumped in, raising the water level again by about 10 m further. Now, however, leakage from the borehole into the basal system was detected in a slow decline of the water level. Then, a few minutes later, the hole broke through abruptly to the basal system and the water level dropped rapidly (in 2 minutes) back to 107 m, the same level reached initially by water upflow from below. The water levels in three subsequent boreholes drilled later nearby (98-2, 98-3, 98-6) dropped to the same 107 m water level after breakthrough.

The experiment in hole 98-1 shows that there exists, prior to any modification by hot-water drilling, a basal water system capable of delivering a substantial quantity of water before any water has been introduced into it from a borehole. The system has, at least locally (over a horizontal distances of at least 21 m), a well defined water pressure, which is maintained on water input or withdrawal. The rise time of 3 minutes corresponds in the gap-conduit model to a gap of 1.8 mm. Although strictly these conclusions apply only to the study site on Ice Stream D, it seems likely that they are valid broadly for the ice streams, which, as noted above, show similar breakthrough-with-water-level-drop behavior in all boreholes studied thus far.

Aside from the anomalous hole 88-2 (E & K, p. 210), the only exceptions to this are two boreholes in which unsuccessful attempts were made to do the experiment that was later successfully carried out in hole 98-1 as described above. The two holes, 95-3 and 96-3, showed no indication or almost no indication of breakthrough. In Section 4.6 this is interpreted for hole 95-3 as an indication that the borehole bottomed in frozen till. An alternative interpretation, applicable also to borehole 96-3, is that when the drill reached the bottom, the borehole water level, which had been drawn down as far as possible in advance, was the same or nearly the same as the water level of the basal system, and for this reason hydraulic connection did not occur. It is possible that a certain overpressure at the base of the borehole water column is necessary to make connection with the basal water system, perhaps by breaking through a hydraulic barrier. Alternatively, because of the draw-down it is possible that a hydraulic connection could have been made between the borehole and the basal system without being detected from a drop or rise in water level. In hole 95-3 there was no change in water level (at 107 m), and in hole 96-3 there was a slow drop of 3 meters (in 36 minutes, to water level 114 m), which may indicate a weak breakthrough to a basal system with water level 114 m. What happened after the possible initial connection is noteworthy. Connection (if any) was lost (in 2 to 20 hours), and by pumping water into the borehole the water level was raised to 57 m in hole 95-3 and to 94 m in hole 96-3. At these levels a substantial overpressure was being applied to the basal zone: expressed as a difference in hydraulic head, the overpressure in hole 95-3 was 107-57 = 50 meters and in hole 96-3 it was 114-94 = 17 meters. The experience assembled in Table 1 shows that breakthrough has occurred with an overpressure as low as 14 meters (borehole 95-2). (Overpressure is the difference between the "pre-breakthrough" and "post-breakthrough" entries in Table 1.) Hence breakthrough is expected, but it did not occur. This could be explained by a frozen bed in both boreholes. But it seems quite unlikely that, out of the many boreholes that have been drilled in the ice streams, a frozen bed would happen to be encountered by just the two boreholes in which during drilling the borehole water level was drawn down to the water level of the basal water system. Instead, the apparent lack of initial breakthrough under these conditions, and/or the lack of later breakthrough when the borehole water level was raised above an overpressure of 14 m, should probably be recognized as a special and peculiar property of the basal water system, perhaps related to the temporary loss of connection that closely followed the initial breakthrough in hole 98-1 as described earlier.

The above conclusion must be qualified by recognition that the two piston cores from borehole 95-3, in which the sediment was clearly sorted and graded, strongly favor the frozen-bed interpretation, because such sediment has otherwise been recovered only from boreholes that bottomed in frozen till (Section 4.5). (See also the discussion in the second-to-last paragraph of Section 6.4.) A small piston core was obtained from borehole 96-3, but because of wash-out by water escaping from the core barrel the sediment was not suitable for comparison with hole 95-3.

The two alternative interpretations of boreholes 95-3 and 96-3, discussed here and in Section 4.5, illustrate the contradictory character of some of the evidence on the basal zone from borehole observations.

7.2 Water-level Oscillations

The water-level drop curves on breakthrough for holes 98-2 and 98-3 show a new feature, a damped oscillation at the end of the drop (Figure 20). The oscillation in hole 98-2 had a period of 1.3 minutes, an initial amplitude of about 4 m (peak to peak), and a decay to the noise level of ~2 m in about 3 minutes. In hole 98-3 the period was 1.6 minutes, initial amplitude 5 m, and decay time about 6 minutes. It seems that what is happening in the oscillation is a seiche-like movement of water back and forth between a pair of closely spaced boreholes open to the atmosphere and connected via a basal water conduit (borehole spacing 2.5 m for pair 98-2 plus 98-1, and the same for pair 98-4 plus 98-3). A dynamical model of such a system [*Kamb*, unpublished] accounts for an oscillation period of about 1.5 minutes if the basal conduit is a till-ice gap of thickness about 2.5 mm.

The occurrence of well-defined waterlevel oscillations in Ice Stream D but not in any of the boreholes in Ice Streams B or C may represent a difference in the nature of the basal water system in these ice streams, or it may alternatively reflect a rather narrow limitation on the range of conditions under which the oscillation can occur, which is what is indicated by the model.

7.3 Water-level Drop Times

Of the eight WLDT's measured in Ice Stream B (Table 1), seven were in the range 2-3 minutes while the remaining one was about 5 minutes (this omits hole 95-4, whose WLDT was only crudely estimated). (Also not included in these WLDT statistics are holes 88-2 and 95-3, which had very anomalous behavior—see Section 7.1 and E & K, p. 210.) For Ice Stream C the corresponding WLDT's are, out of twelve measured, five in the range 2-3 minutes, while the remaining seven are 5 minutes to 30 minutes or even longer. Hole 96-4 is included in the latter group because, although its water level started dropping with a time constant of 2.5 minutes, when it reached a depth of 75 m the water system changed in a way that introduced complications into the drop curve (Figure 21a) and lengthened the WLDT to about 30 minutes.

Water-level drop behavior somewhat similar to 96-4, but even more striking, was shown by borehole 96-12, which was drilled in the middle of the fossil shear margin between Ice Stream C and Ridge B-C. The initial part of the drop curve (Figure 21b) has a quasi-exponential shape with time constant of about 1 *hour*, which is highly abnormal. Below a depth of 90 m the drop was further delayed, with complications somewhat resembling those of borehole 96-4, lengthening the overall WLDT to about 5 hours—extremely abnormal. In terms of this very long WLDT, the basal water system under the shear margin can be recognized as transitional in character between the active ice streams (WLDT 1-3 minutes) and the non-streaming ice sheet, which has no basal water system and in effect an infinite WLDT. The basal water system under the central part of Ice Stream C shows a suggestion of this transitional character in terms of the WLDT statistics discussed above and the anomalous water-level drop curve of hole 96-4.

Further discussion of the significance of the WLDT is in Section 8.2.

7.4 Basal Water Pressures and Effective Pressures

Now that the existence of a basal water system with a locally well defined pressure has been established (Section 7.1), it is necessary to reconsider in this new light the problems posed for concepts of the basal water system by several aspects of the borehole observations of basal water pressures and the effective pressures derived from them (Section 3.2):

(1) The large scatter (± 6 m) in individual water-level depths, corresponding to the scatter of $\pm\ 0.7\times10^5$ Pa in effective pressure values (Section 3.2), implies the presence of large, spatially variable water-pressure gradients that would produce impossibly large, spatially variable local water fluxes in a gap-conduit water system of the type contemplated (E & K, Section 9d).

(2) Negative effective pressures, of which nine are indicated, ranging from -0.1 to -1.0×10^5 Pa (Table 1), are physically impossible in a steady-state gap-conduit system. Negative effective pressure is involved in the gap-opening model considered by E & K (Section 9a) but this represents

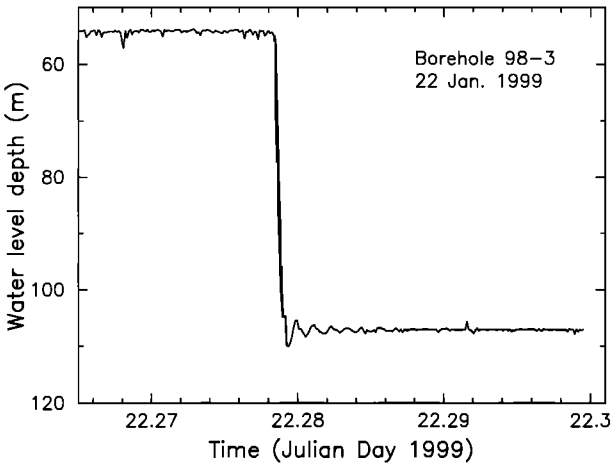

Figure 20. Water-level drop in borehole 98-3, Ice Stream D, showing damped oscillation of the water level about the 107 m depth.

a situation that could not arise in the natural system and if created artificially is a transient that would not long persist. To some extent the negative values may be due to systematic error in the calculation of the ice overburden pressure (E & K, Section 4).

(3) Positive effective pressures range up to + 1.7×10^5 Pa, which, with the till's internal friction of 0.44 (Section 6.3), would result in till strengths of up to 0.75×10^5 Pa, much larger than the 1-5 kPa from direct measurement (Sections 6.1, 6.2, and 6.4). From theoretical considerations of till-lubricated ice-stream motion (Section 9.2) the till strength should be equal to the basal shear stress, and the basal shear stress should be less than or equal to the driving stress $\rho g h \alpha$. The latter is 0.15×10^5 Pa (for $\alpha = 0.1°$), which is considerably smaller than the 0.75×10^5 Pa till-strength value noted above. Thus there is a contradiction. Perhaps the water-level measurement error is considerably greater than the estimated ±1 m, but that seems unlikely, especially for the sounding-float measurements, to which the pressure-transducer measurements are tied. The above contradiction would be avoided if the ice-stream motion were due to basal sliding sensu stricto, without till lubrication, in which case the till shear strength would have to be larger than the basal shear stress, and a basal sliding mechanism furnishing the observed motion would have to be in operation at the effective pressure level inferred from the observations. A contradiction between the measured till strengths and the strength calculated from the effective pressure would remain.

It has been suggested that the actual ice overburden pressures differ considerably from the calculated values, such that the actual effective pressures are all practically zero. The cause of the required sharp local variations in overburden pressure is not explained and raises mechanical questions. Moreover, with this explanation, the spatially varying water pressures are retained, so that problem (1) remains a problem.

(4) In some cases nearby boreholes show the same or nearly the same water levels, as is expected if the boreholes tap into the same basal conduit (E & K, pp. 209, 215). This seems to be the case for boreholes 96-3, 96-4, 96-8, and 96-13, which were within 50 m of one another and had water level depths 112 ± 2 m, and perhaps also for boreholes 96-9, 96-10, and 96-11, again within 50 m of one another, with water levels of 118 ± 4 m. (The water level depths are indicated in the borehole map, Figure 3.) But the expectation is shattered by holes 96-1 and 96-2, only 2.5 m apart but with water levels of 102 and 117 m, and

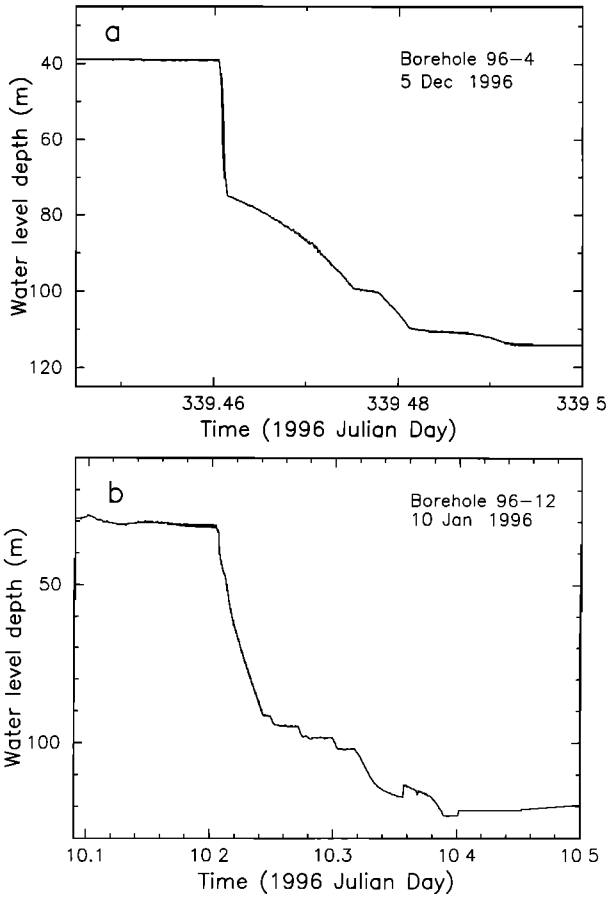

Figure 21. Abnormal water-level drop curves in Ice Stream C: (a) in borehole 96-4; (b) in borehole 96-12, drilled in the center of the fossil marginal shear zone between Ice Stream C and Ridge B-C.

also by holes 96-5 and 96-6, again 2.5 m apart, with water levels of 107 and 96 m.

(5) The cause(s) and significance of the long-term variations in basal water pressure (and/or till pore pressure), which are seen in Ice Stream C (Figure 5) as well as in Ice Stream B (E & K, Section 5), are not known. Likewise for the diurnal variations (Figure 5b; E & K, p. 216).

(6) The problem of explaining the results of the pressure-pulse-propagation experiment in Ice Stream B (E & K, Section 8) is reraised by the newer observations (Section 7.1).

The above problems, and others pointed out here and there throughout this paper, such as the lack of a strong physical distinction between Ice Stream C and Ice Streams B and D (Section 8), seem to be the observationalist's counterpart to the theoretician's "as yet inscrutable property of the bed that escapes our understanding" [*MacAyeal et al.*, 1995, p. 262].

7.5 "Canal" System?

For reasons based on problem (1) above, E & K (Section 9e) concluded that the basal water system must involve localized conduits ("canals") that are ~ 1 m in width and ~ 0.1 m in thickness and that carry most of the water flux of the system. An effort has been made to find such a conduit by searching via boreholes for gradients in basal water pressure and in WLDT and/or time constant T. Holes 95-9, 95-10, and 95-11, for example, were drilled with this objective. However, no observational indication of a canal conduit has been found. This is perhaps not surprising, since basal conduits are difficult to find by means of boreholes in temperate glaciers.

The potential complexity of the basal water conduit system is well illustrated in the flume experiments of *Catania* [1998], which produced a complex variety of braided and unbraided channels and sheet flows at the sediment-"ice" (actually plexiglass) contact, with average channel width dimensions from 0.8 to 18 cm and average depth dimensions from 0.5 to 15 mm. The depth dimensions are roughly comparable to those found here for the gap-conduit model (Sections 7.1, 7.2).

7.6 Basal Melting and/or Freeze-on

A fundamental aspect of the basal water conduit system is the magnitude of the water sources or sinks that feed or deplete it—by basal melting, freeze-on, or seepage of water out of or into the till. A related aspect is the magnitude and time derivative of water storage in conduits or chambers of the water system and in the till. These quantities are of course linked by the water transport flux in the system and by the flux gradients. They are also tied to the thermal conditions at the base of the ice stream, specifically the geothermal gradient, the shear heating due to basal sliding or basal till deformation, and the vertical temperature gradient in the basal ice. Except for the latter, which is discussed in Section 3.1, observational constraints on these quantities are few and are greatly needed to provide a firmly-based concept of the nature and functioning of the basal water system.

Measurement of the transport velocity in the basal water system (E & K, Section 7) has been repeated subsequently once (in boreholes 92-1, 92-2, and 92-4) with similar results, which are compatible with the gap-conduit model with a gap thickness of about 4 mm (E & K, p. 222).

7.7 Detection of Basal Freeze-on

Because in hot-water drilling the breakthrough from ice into unfrozen till seems always to be accompanied by an immediate onset of water-level drop, and because when the drill encounters coarse rock debris in the ice the rate of drill progress is slowed, there is a possibility of detecting a thin layer of frozen till at the bottom of the ice from a time delay between a premonitory slowing of drill advance and the onset of water-level drop. Such a delay appears to have occurred in four boreholes in Ice Stream C and two holes in Ice Stream B. Figure 22 shows an example of the observations. The borehole water-level depth and the drilling-hose load (tension) are plotted as a function of time starting about 80 minutes before breakthrough in hole 95-5. The beginning of the premonitory slowdown is marked with a downward-pointing arrow in the figure. The drill slowdown appears as a progressive decrease in drilling load because the drilling hose was being paid out from the surface at a steady rate, and when the drill advances more slowly than the hose is being paid out, the stretch and hence the tension in the hose decreases. Six minutes after the onset of slowdown, breakthrough began as marked with the upward-pointing arrow in the figure. Breakthrough is indicated by the rapid drop in water level and the sudden increase in drill load caused by the drill being pulled down by the downrushing water.

An alternative interpretation of the premonitory slowdowns, which avoids the possible implication of basal freeze-on under Ice Streams B and C, is to attribute them to delay in the process of hydraulic connection from borehole to basal water system. That such delay can occur seems to be demonstrated by anomalous borehole 88-2, in which the connection was delayed 9 hours after the drill

reached the bed as indicated by cessation of drill advance (E & K, p. 210).

8. COMPARISON OF ICE STREAM C WITH ICE STREAMS B AND D

The study of Ice Stream C was undertaken with the idea that, since rapid streaming flow in C stopped about 150 years ago [*Shabtai and Bentley*, 1987; *Alley and Whillans*, 1991; *Retzlaff and Bentley*, 1993; *Smith et al.*, 1999] whereas in B and D (called collectively "B/D" below) the flow continues vigorously, a comparison of C with B/D should reveal which physical factors are responsible for the rapid motion or its cessation. The information in Sections 3-7 has been gathered with this objective in mind. What emerges is that, although C and B/D are quite different in terms of flow velocity (ca. 0.04 m d^{-1} vs. ca 1 m d^{-1}), these ice streams look largely the same in terms of the possibly controlling parameters revealed by the borehole measurements. However, in the data there are a few hints of differences. The similarities are first summarized, and then the hints of differences are considered in some detail.

8.1 Similarities

Ice Stream C has a basal water system generally similar to those of B/D in terms of the breakthrough phenomenon (Sections 7.1, 7.3) and the behavior of the borehole water level in pumping tests (E & K, Section 6). This is somewhat surprising, because drilling in the ice sheet outside the ice streams (including C) has not produced breakthroughs or other indications of a basal water system (Section 4.5; E & K, p. 210). Thus, one might have expected that, as a stopped ice stream, C would be frozen to its bed and would lack a basal water system.

The basal water pressure measured under Ice Stream C corresponds to an average effective pressure of 0.2×10^5 Pa while under B the average is 0.6×10^5 Pa, and under D, 0.4×10^5 Pa (Section 3.2). The difference is not great except as viewed in the light of Section 7.4, item (3), but the difference goes the wrong way, tending to promote more rapid motion in C rather than in B/D. Thus an effective-pressure increase suitable for shutting down the streaming motion of C is not observed. Possibly this is because the large scatter of the individual water-pressure values ($\pm$ 0.7×10^5 Pa) hides a small but real difference between the effective pressures under C and B/D.

Ice Stream C is underlain by weak unfrozen till that is similar to the till under B/D in porosity (Section 4.2) and in general lithological and sedimentological characteristics (Section 4.1) including the presence of diatoms. Four of the Ice Stream C cores showed some evidence of having been slightly disturbed by winnowing and resedimentation, as could be expected from the water-jet action of the drill (Section 6.4, fourth paragraph).

The estimated thickness of till based on till core lengths is distinctly smaller for C ($\geq$0.3 m) than for B ($\geq$ 3 m at Up B; $\geq$ 0.7 m at New B), but these estimates cannot be relied upon because drilling-penetration tests indicate much larger thicknesses ($\geq$ 5 m).

The above situation, in which there is a strong difference in streaming velocity between Ice Stream B and C without a strong difference in physical conditions that could be responsible, is a curious counterpart to the situation encountered within Ice Stream B, in which there were rather large time-variations in basal water pressure without a detectable variation in streaming velocity (E & K, p. 217].

8.2 Differences

Although borehole breakthrough behavior in C and B/D is similar in a general way, there is a statistical tendency for the water-level drop time (WLDT) to be longer in C, as discussed in Section 7.3. The tendency manifests itself in two ways: (1) In B/D, water-level drop curves of the normal quasi-exponential form have WLDT's mostly in the range 1-3 minutes, whereas in C more than half of them are in the range from 5 to 30 minutes. (2) In C, two drop curves that begin in quasi-exponential form undergo a change partway down into more complicated, segmented forms that substantially lengthen the drop time (Figure 21). Borehole 96-12 is a particularly special case, first because of its extremely long WLDT of 5 hours (Figure 21b), and second because of its location, in the center of the fossil marginal shear zone that lies between the main mass of Ice Stream C to the north and the B-C Ridge to the south. Because of this location, the breakthrough behavior of borehole 96-12 is probably indicative of the character of a basal water system that is intermediate between streaming and non-streaming conditions.

The significance of the WLDT as a parameter in comparing the basal water systems of Ice Streams C and B/D is that it can be regarded as an inverse measure of the water throughput capability of the system. The related exponential time constant (T in Table 1) is an inverse measure of the gap width in the gap-conduit model (E & K, Section 9a), and consequently is also a measure of

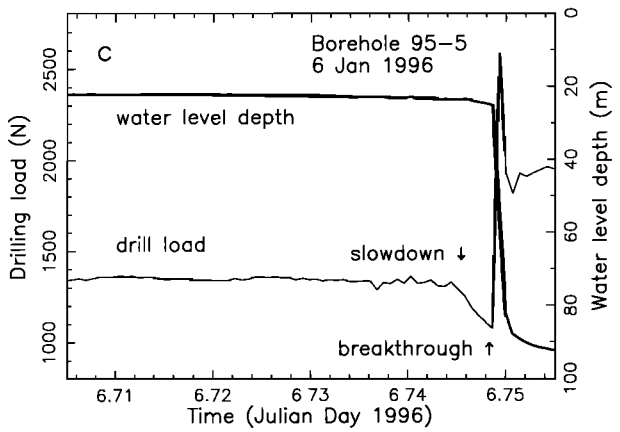

Figure 22. Drilling record showing preliminary slowdown in borehole 95-5 beginning approximately at the downward-pointing arrow. The thin line is the drilling load record, and the heavy line is the borehole water-level record, which confirms the identification of breakthrough in the drill-load record as indicated by the upward-pointing arrow. The abrupt rise in drilling load (hose tension) is caused by downrush of water in the hole at breakthrough.

throughput capability. Why should throughput capability be linked to ice streaming? If ice streaming is associated with enhanced basal melting, then enhanced throughput is necessary to carry the increased basal water flux associated with streaming. Enhanced throughput might be achieved by enlargement of the basal conduit system, perhaps by a type of basal cavitation, or it might be achieved by increased basal water pressure, which in turn might lead to enhanced cavitation or to the type of flow instability considered by Kamb (1991). Why should the indication of throughput capability be statistical? Perhaps this is related to the statistical character of the basal water systems in temperate glaciers, such as Columbia Glacier [*Kamb et al.*, 1994, Section 5].

A related difference between the basal water systems of Ice Streams B and C is the behavior of the pressure-pulse-propagation tests (Section 7.1), which implied low throughput capability for B and relatively high throughput for C, in contradiction to the interpretation of the WLDT's above. This contradiction illustrates the difficulty in reaching a clear and unambiguous understanding of the controls on the ice streaming mechanism.

Torvane data (Section 6.4) indicate that the in-situ strength of the till under Ice Stream C is about 5 kPa, which is about 3 times greater than that under B/D (about 2 kPa/1 kPa). This difference appears to be significant in explaining the slowing of Ice Stream C, according to the theory of ice-stream mechanics discussed in Section 9.2.

8.3 Role of Basal Freeze-on

Although unfrozen till is obtained by piston coring from the base of Ice Stream C, as it is from B/D, there is a possible indication in four Ice-Stream-C boreholes (96-1, 96-6, 96-9, and 96-12) that the drill encountered and drilled through a thin layer of frozen basal till between clean basal ice above and unfrozen till below. This is discussed in Section 7.7. It suggests that a small amount (~ 0.5 m?) of till freeze-on has occurred relatively recently at the base of Ice Stream C, perhaps during the 150 years since the ice stream shut down. The freeze-on interpretation would be more secure if all 10 boreholes with adequate drilling records confirmed it. A similar indication of basal freeze-on has also been encountered in two boreholes in Ice Stream B (holes 95-4 and 95-5), which blurs a possible distinction between Ice Stream B and C as far as the occurrence of basal freeze-on is concerned. However, a statistical distinction can perhaps be recognized, in that the possible freeze-on was encountered in 4 boreholes out of 13 in Ice Stream C but in only 2 out of 29 in Ice Streams B/D. (The 2 in B/D should probably count as only 1 because the two holes are only 15 meters apart.)

If the till layer under Ice Stream C is thin (Section 4.3), a relatively small amount of basal freeze-on might be sufficient to bridge the interval from the top of the till to the bedrock, producing the situation wherein the ice stream becomes frozen to its bed and streaming flow stops. However, this situation is ruled out by the fact that unfrozen till was consistently encountered below the inferred thin basal layer of frozen till. Thus the freeze-on probably is not directly responsible for the stopping of the ice stream by freezing to the bed, but is instead probably a collateral consequence of other changes that are responsible for the stopping (see Section 9.2).

Since the freeze-on process appears to be patchy and discontinuous (apparently detected in 4 boreholes out of 10 in Ice Stream C), one might be tempted to suggest that a scattering of sticky spots at patches where the ice is frozen to its bed is sufficient to arrest the rapid motion of the ice stream while intervening unfrozen-bed areas are able to house an interconnected basal water system. But no evidence supports such a model, because, as noted in the last paragraph, the four detected patches of freeze-on were not frozen to the bed (with possible exception of the patch encountered by borehole 96-1, for which no piston core was obtained).

The amount of freeze-on that could have accumulated in the 150 years since Ice Stream C stopped streaming can be estimated from the temperature gradient in the basal ice (52 C km^{-1}) and the geothermal heat flow (70 mW m^{-2}),

assuming that these quantities did not vary appreciably during the 150 years and that basal shear heating was negligible once the ice streaming stopped. (The geothermal heat flow was measured at Siple Dome by *Engelhardt* [2000] and this value is assumed valid under Ice Stream C.) The calculated freeze-on rate is 4.5 mm of ice per year, giving a total of 67 cm in 150 years. This figure should be increased by a factor of about 1.7 to include the frozen till's content of coarser rock particles (excluding clay). Thus the thickness of frozen-on till should be ~ 1 m. It seems possible that the hot water drill could penetrate through a meter of frozen till, provided that the rock clasts encountered are not too large or numerous.

Related to the possible observation of basal freeze-on under Ice Stream C is the observation of a basal temperature 0.35 degrees C below the freezing point (Section 4.6), which contrasts with the near-melting-point condition at the base of Ice Stream B (Section 3.1). According to the interpretation in Section 4.6, the 0.35 C below freezing implies that the melting isotherm lies 7 m below the bottom of the boreholes, but this again is contradicted by the observed breakthrough to a basal water system in all Ice-Stream-C boreholes (except 96-3, discussed in Section 7.1) and by the recovery of unfrozen till cores from the bottom of several of these boreholes (Table 2). At the same time it is difficult to ascribe the sub-freezing observation to measurement error, since the thermistor calibrations show measurement accuracy and long term drift-free precision of ± 0.02 C, and since two independent sets of measurements (in holes 96-2 and 96-12) agree on the 0.35-degree subfreezing basal temperature.

There is a possibility that the 0.35 C discrepancy is due to lowering of the melting point by dissolved impurities (air and salts) in the basal water. For example, if the water were saturated with air at the ambient pressure, the melting point would be depressed to –1.0 C, only 0.1 degree above the measured basal temperature of –1.1 C. Also, an 0.35 degree depression of the melting point would be effected by a salt concentration of 0.56% (compare with sea water salinity of about 3.5%). Basal freeze-on would tend to concentrate impurities in the residual water, because in the freezing process ice rejects impurities. This explanation of the 0.35 C discrepancy fits qualitatively with the theory of ice-stream mechanics discussed in Section 9.2.

9. THEORY

In a broad way the features of the ice-stream basal zone observed in the work summarized here appear to agree with conceptions held and assumptions made in recent and current theoretical treatments and numerical models of the West Antarctic ice streams. But there is a divergence of views on some points. I will not try to make an exhaustive survey of these, but will briefly discuss two that seem particularly important.

9.1 Viscous vs. Treiboplastic Flow

The largest and most fundamental area of difference is in formulation of the basal boundary condition for till lubrication of ice-stream motion. The central feature of this condition is the rheology of the till (Section 6.6). The till has been widely treated as a viscous or quasiviscous fluid with linear or slightly nonlinear flow law of the standard type (13) in which n is 1 or slightly greater than 1. The results in Section 6.6 indicate on the contrary that the till behaves rheologically as a soil or granular solid, with treiboplastic (Coulomb-plastic) failure law (3). Most of the mechanical tests on the till show a small but definite strain-rate dependence of the strength, and if this is incorporated into the rheological formulation the failure law becomes a flow law of power-law type (15), in which the exponent n is a large number ~ 40. Such a rheology is probably more convenient for numerical modeling of ice stream flow than is the perfect treiboplastic failure condition, for which a flow law cannot be written. The large value of n means that there is a great difference in flow-law nonlinearity between the till (highly nonlinear) and the linear viscous or slightly nonlinear quasiviscous rheologies that have been assumed in ice-stream modeling. It seems likely that ice-stream models with a basal boundary condition formulated from the highly nonlinear flow law will be quite different from models based on the linear or only near-linear (13) with n equal to 1 or slightly greater. An example of an ice-stream model based on (13) with large n is the model of Kamb (1991), which shows a type of prompt instability that is an immediate consequence of the flow-law nonlinearity and that has not been recognized in ice-stream models based on linear or slightly nonlinear rheologies.

While the high nonlinearity of the treiboplastic rheology of granular materials seems now well established for ice-stream till, Hindmarsh (1997) has put forward a theory that as the dimensional scale of deformation increases, till rheology undergoes a transition from plastic to viscous at a scale much larger than the grain scale but smaller than the scale of deformation in large ice-sheet models. Above the "cross-over scale" between plastic and viscous deformation the till is apparently supposed to flow as a viscous liquid. The argument for this idea is that "large scale modelling studies using a viscous model of till

deformation have been reasonably successful in predicting the geological consequences of ice sheet action". However, I do not see a physical basis for the idea. Hindmarsh goes to some length to build one from a concept of small-scale plastic failure events summing over a larger scale to give viscous flow, but "the key theoretical problem which has yet to be solved is how multiple small scale failure events combine into a viscous type flow" [*Hindmarsh*, 1997, p. 1039].

9.2 The Undrained-treiboplastic-bed Model

On the basis of concepts of the ice-stream basal zone some of which are discussed in the present paper, Slawek Tulaczyk has formulated a new theory of ice-stream mechanics, which shows in a simple way how the physical components of a conceptualized ice-stream mechanism operate and interact to produce a system with well defined stable and unstable states (Tulaczyk, 1999, Chapter 6). He calls the theory the undrained-plastic-bed model (UPB). Only its basis and major features can be sketched here, but a full treatment is available in *Tulaczyk et al.*, (2000b).

The UPB theory describes a till-lubricated model of the ice stream mechanism in which the till behaves rheologically as a treiboplastic material. A straight ice stream of thickness h and width $2w$, with uniform surface slope α and driving stress $\tau_D=\rho g h\alpha$, overlies an unfrozen basal till layer of thickness l, and flows in rectilinear, channel-type flow through an ice sheet of the same h and α. In the spirit of the simplest model of channel flow of glaciers [*Nye*, 1965], all across-slope cross sections of the ice stream are assumed to look the same and behave in the same way (no along-flow variation). The ice stream is supported against the down-slope component of gravity by marginal shear stress τ_M and by uniform basal shear stress τ_B, which is equal to the shear strength τ_f of the till, so that the till layer accommodates an arbitrarily large or small ice motion by shearing at a particular yield stress $\tau_f=\tau_B$. This behavior represents treiboplastic rheology of the bed. The ice-stream flow velocity u is a known function of τ_D, which drives the ice forward, and τ_B, which resists the forward motion. The combined action of u and τ_B generates a frictional heating in the amount $u\tau_B$ (per unit area) within the till. To this is added the geothermal heat flow q_G, less the heat conducted upward into the ice q_I (in response to the vertical temperature profile (Figure 4)), giving a net basal heat budget in the amount $u\tau_B+q_G-q_I$. This heat produces either basal melting at a rate $\dot{m}$ (positive) or basal freeze-on at a rate $\dot{m}$ (negative) at the till-ice interface (Section 7.6). The basal melt water seeps into storage in the till, or else water seeps out of the till to freeze onto the bottom of the ice, as required by $\dot{m}$.

The assumed equality of the basal melting rate and the rate at which water goes into or out of storage as pore water in the till represents the condition of an undrained bed, for which arguments have been given by *Tulaczyk* [1999, p. 5-31]. If the equality did not hold, water would either have to enter or leave macroscopic storage chambers in the basal water system, for which there is no provision in the model, or else water would have to be added to or subtracted from the water in longitudinal transport in the basal water system, violating the assumption of no along-flow variation. The undrained-bed condition seems perhaps questionable in view of the existence proof for the basal water system (Section 7.1), but it should be realized that there is as yet no actual field evidence for the role of the basal water system in ice stream flow. Also it should be appreciated that the model is purposely made as simple as possible, so that the possible complexities involved in water storage in macroscopic chambers (such as a basal gap) and in water transport variably along the length of the ice stream are intentionally avoided at this first step in modeling. In this model the role of the basal water system is that it provides a basis for control of ice-stream motion via the effect of the basal water pressure on the till strength τ_f, which is constant along the length of the ice stream. *Tulaczyk et al.* [2000b] show that the undrained-bed condition can be relaxed, subject to certain assumptions, without a large modification in the formulation or results of the theory.

The change in water storage in the till is a change in the till water content and hence in the till's void ratio e (Section 4.2), at a rate $\dot{e}$ that is proportional to $\dot{m}$. The strength of the till is an exponential function of e (another feature of treiboplasticity, discussed in Section 6.5), so that $\dot{e}$ causes the strength to change at a calculable rate $\dot{\tau}_f$, and τ_B changes at the same rate $\dot{\tau}_B=\dot{\tau}_f$. Thus, starting with a given value of basal shear stress $\tau_B=\tau_f$, we have a corresponding ice-stream flow u, a corresponding shear heating $u\tau_B$, a corresponding net basal heat budget $u\tau_B+q_G-q_I$, a corresponding basal melting rate or freeze-on rate $\pm\dot{m}$, a corresponding rate $\dot{m}$ of water uptake by the till or release from the till, a corresponding time rate of change $\dot{e}$ in the void ratio of the till, and finally, a corresponding rate of change $\dot{\tau}_f=\dot{\tau}_B$ via the exponential dependence of τ_f on e.

Formulated explicitly, this chain of correspondences is as follows. It starts with a relation derived by *Raymond* [1996, equation (39)] between τ_B and the ice-stream centerline basal velocity u:

$$u = \frac{1}{2} A (\tau_D - \tau_B)^3 w^4 h^{-3} \quad (17)$$

where A is the constant in the standard $\dot{\gamma} = A\tau^3$ flow law for ice. Because the centerline velocity is fairly representative of the velocity over most of the width of the ice stream [*Echelmeyer et al.*, 1994, Figure 4], (17) is taken to apply to the motion of the ice stream as a whole. The basal melting rate is then

$$\dot{m} = (u\tau_B + q_G - q_l) H^{-1} \quad (18)$$

where H is the latent heat of melting per unit volume. Storage of the melt water in the till requires

$$\dot{e} = (1+e)\dot{m} l^{-1} \quad (19)$$

where l is the till thickness. The exponential relation (4) between e and τ_f can be simplified to

$$\tau_f = a \exp(-be) \quad (20)$$

where a and b are aggregations of the constants in (4). To calculate the effect of $\dot{e}$ on τ_f, (20) is differentiated with respect to time:

$$\dot{\tau}_B = \dot{\tau}_f = -\dot{e}ab \exp(-be) = -b\tau_B\dot{e} \quad (21)$$

Equations (17)-(21) provide the basis for understanding how the simple till-lubricated ice stream of the UPB model operates. In general, a given τ_B corresponds to a rate of change $\dot{\tau}_B$ via these relationships. Of particular interest are steady states of the system, which can persist over time. They are states for which $\dot{m}$ (and hence also $\dot{e}$ and $\dot{\tau}_B$) is 0. Such states can exist only if $q_G - q_l$ in (18) is negative, since $u\tau_B$ is inherently positive (or 0). This condition is very likely satisfied in the ice streams, because the temperature gradient in the deep ice is abnormally large ($\geq$40 C km^{-1}: Section 3.1). As shown in Figure 23a, for a range of values of $q_G - q_l$ there are two steady states. One of these states is stable and the other is unstable. This is shown by linear stability analysis as follows.

Let τ_B^* be a value of τ_B for which there is a steady state, $\dot{\tau}_B^* = 0$. Consider states for which τ_B differs only slightly from τ_B^*, and let $\Delta\tau_B = \tau_B - \tau_B^*$, a small quantity. Its time derivative $\Delta\dot{\tau}_B$ equals $\dot{\tau}_B$, because $\dot{\tau}_B^* = 0$. It can be shown that $\Delta\dot{\tau}_B$ varies linearly with $\Delta\tau_B$ for small $\Delta\tau_B$, so that one can write

$$\Delta\dot{\tau}_B = \frac{\partial\Delta\tau_B}{\partial t} = p\Delta\tau_B \quad (22)$$

where p is a constant. The solution of (22),

$$\Delta\tau_B = D \exp(pt) \quad (23)$$

(where D is an arbitrary constant), implies that the state is stable if $p < 0$ and unstable if $p > 0$. To determine p in (22), take the derivative of $\dot{\tau}_B$ with respect to τ_B and then set $\tau_B = \tau_B^*$. For differentiation, $\dot{\tau}_B$ as a function of τ_B can be obtained by starting with (21) and introducing successively (19), (18), and (17). One obtains finally

$$p = -b\frac{1+e}{2H} A \frac{w^4}{h^3} \tau_B^* (\tau_D - \tau_B^*)^2 (\tau_D - 4\tau_B^*) \quad (24)$$

Of the factors in (24), the only one that changes sign in the interval $0 < \tau_B^* < \tau_D$ is $(\tau_D - 4\tau_B^*)$, so it governs the stability/instability of the system in the state $\tau_B = \tau_B^*$. It is stable if $\tau_B^* < \frac{1}{4}\tau_D$ and unstable if $\tau_B^* > \frac{1}{4}\tau_D$. The dividing line between stable and unstable states, $\tau_B^* = \frac{1}{4}\tau_D$, is at the maximum in the curve of basal melting $\dot{m}$ as a function of τ_B (Figure 23a). The state to the left, at smaller τ_B, and with larger flow velocity u as shown in Figure 23b, is the stable one. It represents a rapidly flowing ice stream, as can be seen from magnitudes of the velocities along the curve $u(\tau_B)$ in Figure 23b. The state to the right, at larger τ_B and smaller u, is unstable. If perturbed toward smaller τ_B the system would move on over to the stable state on the left, as the arrow labeled $\dot{u} > 0$ in Figure 23b indicates. If perturbed toward larger τ_B the system would move on to the right, until it reaches $\tau_B = \tau_D$, at which point ice streaming has become completely shut down ($u = 0$).

9.3 Shut-down of Ice Stream C

The UPB theory provides a possible explanation for the stoppage of streaming motion in Ice Stream C by

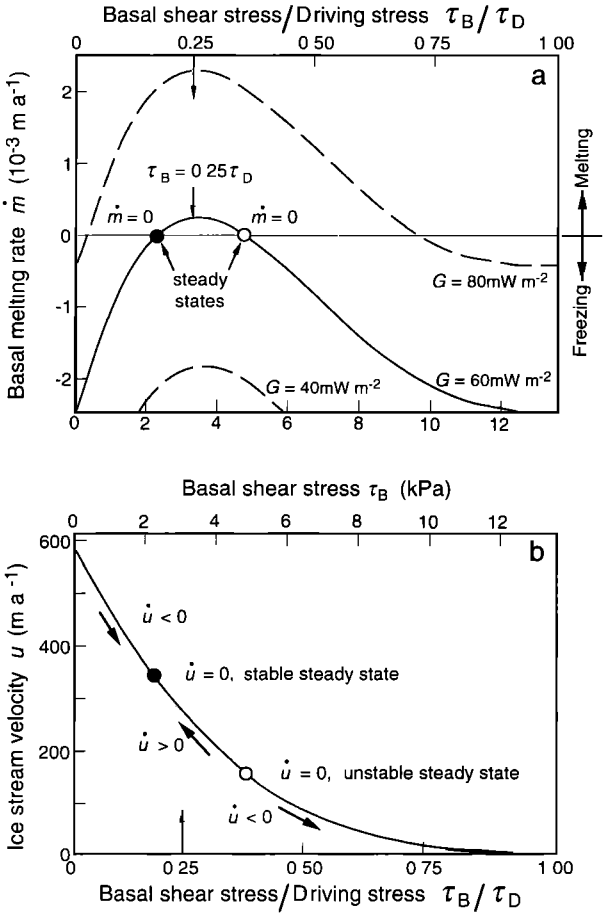

Figure 23. Stable and unstable states of ice-stream motion according to the undrained-treiboplastic-bed theory. (a) Basal melting/freeze-on rate $\dot{m}(\tau_B)$ as a function of basal shear stress τ_B from equations (17) and (18) for three different values of the geothermal heat flux G (called q_G in the text) and fixed basal ice temperature gradient 40 C km^{-1}. Steady states (marked with large dots) occur for $\dot{m} = 0$. The solid dot represent a stable state and the open dot represent an unstable state. (b) Ice-stream flow velocity $u(\tau_B)$ as a function of τ_B, from (17). The two steady states are again shown by dots. An ice-stream system that has been perturbed away from steady state would be represented by a point on the curve $\dot{m}(\tau_B)$ in (a) and the corresponding point on the curve $u(\tau_B)$ in (b). The heavy arrows and the labeling "$\dot{u}>0$" and "$\dot{u}<0$" show the direction in which such a point would move along the curve as time progresses, assuming that finite perturbations behave the same as infinitesimal ones. The sign of $\dot{u}$ is the same as that of $-p\Delta\tau_B$, as follows from (22) and the time derivative of (17). The upper abscissa scale in (a) and the lower abscissa scale in (b) are for τ_B in terms of the ratio τ_B/τ_D, where τ_D is the driving stress, taken to be 13.6 kPa. From *Tulaczyk et al.* [2000b, Figure 6].

linking it to the relatively high shear strength of the till, ~5 kPa, measured with the torvane in Ice Stream C (Section 6.4). The curves in Figure 23 are calculated with a choice of parameters intended to apply the theory to Ice Stream B, but similar results probably apply to Ice Stream C. As shown in the figure, the theory indicates that if during active streaming the basal shear stress is 2 kPa (as it is for Ice Stream B) while the driving stress is 13.6 kPa, with a geothermal heat flux of 60 mW m^{-2} and a basal-ice vertical temperature gradient of 40 C km^{-1}, the streaming flow will be stable at a velocity of about 350 ma^{-1} (to be compared with the actual centerline velocity of 440 ma^{-1} for Ice Stream B). If before shut-down Ice Stream C had τ_B like Ice Stream B, $\tau_B \approx 2$ *kPa*, and if the basal shear stress were then increased to about 5 kPa or slightly greater, the flow would become unstable and the streaming velocity would progressively decrease, ultimately to zero.

The increase in basal shear stress that would bring on the instability and stoppage could result directly from an increase in shear strength of the till. With its internal friction of 0.44 (Section 6.3), an increase in till strength from 2 kPa to 5 kPa could be produced by a reduction of 7 kPa in basal water pressure, resulting in a 7 kPa increase in effective pressure. This is small compared to the ~100 kPa fluctuations in effective pressure observed in boreholes (Sections 2.3 and 7.4), and thus could be masked by these fluctuations. A possible explanation for the reduction in basal water pressure is the "water piracy" theory [*Alley et al.*, 1994] if there exists a suitably connected basal water system in which the piracy could occur.

Figure 23a indicates that as τ_B increases above about 5 k Pa the basal melting rate $\dot{m}$ becomes negative, so that basal freeze-on takes place as the ice stream slows down and becomes stopped. As noted in Section 8.3, this freeze-on may increase the concentration of impurities in the water immediately below the newly frozen-on ice, which may account for the observations in Ice Stream C of basal temperatures 0.35 C below the pressure melting point for pure water (Sections 3.1, 4.6, 8.3). The frozen-on layer may be the thin basal layer of frozen till apparently encountered in four boreholes in Ice Stream C (Section 8.3).

A way in which observation does not conform to UPB theory outlined above is that the measured till strength of ~ 5 kPa corresponds to the theoretical τ_B at the start of the ice-stream shut-down process rather than at or after completion of the process. The theoretically expected τ_B for complete shut-down is instead τ_D, which is taken to be 13.6 kPa in the calculation leading to Figure 23 and is

probably in the range 10-20 kPa for Ice Stream C near Up C. Possibly the measured 5 kPa is low because of mixing of water into the till by the water jet of the drill (Section 6.4).

It appears likely that Ice Stream C is not completely shut down yet, because its flow velocity of 0.04 m d^{-1} at Up C is several times greater than typical non-streaming ice-sheet flow (~ 0.01 m d^{-1}). Thus, its τ_B will not yet have increased fully to τ_D, according to the theory (Figure 23b). This helps to explain why the measured τ_f appears to be less than τ_D. It also explains to some extent why the basal conditions of Ice Stream C are generally similar to those of Ice Streams B and D (Section 8). In particular, it makes understandable the continued existence of a basal water system under Ice Stream C.

9.4 Concluding Remarks

Detailed studies of the ice streams' marginal shear zones have led to the idea that the streaming motion is controlled by the margins and that the basal zone plays only a minor, passive role [e.g. *Echelmeyer et at.*, 1994; *Jackson and Kamb*, 1997, pp. 415 and 423]. Although this is true to an extent, the UPB theory indicates that the basal shear stress has an important influence on the flow, expressed in (17), and determines whether the flow is stable or unstable, as shown in Figure 23. Moreover, one should not lose sight of the fact that the fundamental controlling mechanism that allows an ice stream to attain rapid motion in the first place is the mechanism of basal lubrication, which causes the low basal shear stress. The foregoing paper endeavors to present and interpret observational evidence as to the lubrication mechanism. It shows that while one can claim to understand this mechanism in a general though somewhat vague way, there are a number of detailed aspects for which the observational evidence appears inconclusive or even contradictory and our understanding is inadequate. Thus the ice-stream component of "glaciology's grand unsolved problem"—the West Antarctic Ice Sheet (WAIS) [*Weertman,* 1976]—is as yet only incompletely solved.

Acknowledgments

The results presented here are based on a research program carried out in collaboration with Hermann Engelhardt, whose contributions to it are crucial. I am extremely grateful for his participation and help in countless important ways. Slawek Tulaczyk helped in providing information on the basal till and on his UPB theory. I thank Robin Bolsey for technical assistance of many kinds both in Antarctica and Pasadena. I also thank our colleagues and field assistants, who have helped us so effectively and cheerfully in Antarctica over the years. In rough chronological order: Neil Humphrey, Reed Scherer, Mark Fahnestock, Mark Wumkes, John Chadwick, Jim Berkey, Harold Aschmann, Matthias Blume, Howard Conway, Tom Svitek, Judy Zachariasen, David McKee, Tim Melbourne, Keri Petersen, Patty White, Pavel Svitek, Leanne Allison, Miriam Jackson, Maneesh Sahani, Darius Semmons, Brian Waddington, Sam Webb, Debra Baldwin, Eugene Miya, Katy Quinn, Sabine Schmidt, Keith-Nels Swenson, Marcel Bergman, Sarah Das, Mitch Eaton, Jeff Hashimoto, Rowena Lohman, Beth Pratt, Ginny Catania, Paul Cutler, Elena Hinds, Cheryl Weber, Matt Bachmann, Ben Farrow, Greg Gerbi, Shulamit Gordon, Hans Schwaiger, Erik Mueller, Adam Bucki, Anne Blanchard, Doug Reusch, Sky Colley. Special thanks to Neil Humprhey for building our first piston corer and taking the first till cores, and to Professor Ronald F. Scott (Caltech) and Dr. Less Fruth (Earth Technology, Inc.) for substantial help in carrying out the geotechnical tests of the till. This work was made possible by the support of the U.S. National Science Foundation under grant OPP-9615420 and predecessors.

REFERENCES

Alley, R.B., Water-pressure coupling of sliding and bed deformation: I. Water system, *J. Glaciol., 35* (119), 108-118, 1989a.

Alley, R.B., Water-pressure coupling of sliding and bed deformation: II. Velocity-depth profiles, *J. Glaciol.*, 35, 119-129, 1989b.

Alley, R.B., In search of ice-stream sticky spots, *J. Glaciol., 39*, 447-454, 1993.

Alley, R.B., Progress in ice-stream basal modeling, *Antarctic J. U.S., XXIX* (5), 61-62, 1994.

Alley, R.B., and D.R. MacAyeal, West Antarctic ice sheet collapse: Chimera or clear danger? *Antarc. J., U.S., XXVIII* (5), 59-60, 1993.

Alley, R.B., and I.M. Whillans, Changes in the West Antarctic Ice Sheet, *Science, 254*, 953-963, 1991.

Alley, R.B., D.D. Blankenship, C.R. Bentley, and S.T. Rooney, Deformation of till beneath Ice Stream B, West Antarctica, *Nature, 322*, 57-59, 1986.

Alley, R.B., D.D. Blankenship, C.R. Bentley, and S.T. Rooney, Till beneath Ice Stream B: 3. Till deformation: evidence and Implications, *J.Geophys. Res., 92*, 8921-8929, 1987a.

Alley, R.B., D.D. Blankenship, C.R. Bentley, and S.T. Rooney, Till beneath Ice Stream B: 4. A coupled ice-till flow model, *J.Geophys. Res., 92*, 8931-8940, 1987b.

Alley, R.B., D.D. Blankenship, S.T. Rooney, and C.R. Bentley, Water-pressure coupling of sliding and bed deformation: III. Application to Ice Stream B, Antarctica, *J. Glaciol, 35*, 130-139. 1989.

Alley, R.B., S. Anandakrishnan, C.R. Bentley, and N. Lord, A water-piracy hypothesis for the stagnation of Ice Stream C, Antarctica, *Ann. Glaciol., 20,* 187-194, 1994 .

Anandakrishnan, S., and R. B. Alley, Ice Stream C, Antarctica, sticky spots detected by microearthquake monitoring, *Ann. Glaciol., 20,* 183-186, 1994 .

Anandakrishnan, S., and C.R. Bentley, Micro-earthquakes beneath Ice Stream B and C, West Antarctica: observations and implications, *J. Glaciol., 39*, (133), 455-462, 1993.

Anandakrishnan, S., R.B. Alley, R.W. Jacobel, and H. Conway, The flow regime of Ice Stream C and hypotheses concerning its recent stagnation, Amer. Geophys. Union, this volume, 2000.

Anderson, R.C., Pebble lithology of the Marseilles till sheet in northeastern Illinois, *J. Geol., 63*, 228-243, 1955.

Behrendt, J.C., D.D. Blankenship, C.A. Finn, R.E. Bell, R.E. Sweeney, S.M. Hodge, and J.M. Brozena, CASERTZ aeromagnetic data reveal late Cenozoic flood basalts (?) in the West Antarctic rift system, *Geology 22*, 527-530, 1994.

Bentley, C.R. Antarctic ice streams: a review, *J. Geophys. Res., 92*, 8843-8858, 1987.

Bentley, C.R., Rapid sea-level rise from a West Antarctic ice-sheet collapse: a short-term perspective, *J. Glaciol., 44*, 157-163, 1998a.

Bentley, C.R., Ice on the fast track, *Nature, 354*, 21-22, 1998b.

Bentley, C.R., N. Lord, and C. Liu, Radar reflections reveal a wet bed beneath stagnant Ice Stream C and a frozen bed beneath ridge BC, West Antarctica, *J. Glaciol., 44*, 149-156, 1998.

Berre, T., and L. Bjerrum, Shear strength of normally consolidated clays, *Proc. 8th Int. Conf. on Soil Mech. and Found. Engng., 1*, 39-49, 1973.

Bindschadler, R., The importance of pressurized subglacial water in separation and sliding at the glacier bed, *J. Glaciol., 29*, 3-19, 1983.

Bindschadler R., and T. Scambos, Satellite-image-derived velocity-field of an Antarctic ice stream, *Science, 252*: 242-246, 1991.

Bindschadler R, P. Vornberger, D. Blankenship, T. Scambos, R. Jacobel, Surface velocity and mass balance of Ice Streams D and E. West Antarctica, *J. Glaciol., 42*. 461-475, 1996.

Bindschadler, R.A., R.B. Alley, J. Anderson, S. Skipp, H. Borns, J. Fastook, S. Jacobs, C.F. Raymond, and C.A. Shuman, What is happening to the West Antarctic Ice Sheet? *EOS, 79* (22), 264-265, 1998.

Bishop, W., C.E. Green, V.K. Garga, A. Andersen, and J.D. Brown, A new ring shear apparatus and its application to the measurement of residual strength, *Géotechnique, 12*, 273-328, 1971.

Blake, E.W., U.H. Fischer, and G.K.C. Clarke, Direct measurement of slidng at the glacier bed. *J. Glaciol., 42*, 595-599, 1994.

Blankenship, D.D., C.R. Bentley, S.T. Rooney, and R.B. Alley, Seismic measurements reveal a saturated, porous layer beneath an active Antarctic ice stream, *Nature, 322*, 54-57, 1986.

Blankenship, D.D., C.R. Bentley, S.T. Rooney, and R.B. Alley, Till beneath Ice Stream B: 1. Properties derived from seismic travel times, *J. Geophys. Res., 92*, 8903-8911, 1987.

Blankenship, D.D., R.E. Bell, S.M. Hodge, J.M. Brozena, J.C. Behrendt, and C.A. Finn, Active volcanism beneath the West Antarctic ice sheet and implications for ice-sheet stability, *Nature, 361*, 526-529, 1993.

Blanpied, M.L., T.E. Tullis, and J.D. Weeks, Frictional behavior of granite at low and high sliding velocity, *Geophys. Ret. Lett., 14*, 554-557, 1987.

Boulton, G.S. A paradigm shift in glaciology? *Nature 322*, 18, 1986.

Boulton, G.S., and R.C.A Hindmarsh, Sediment deformation beneath glaciers: rheology and geological consequences: *J. Geophys. Res. 92*, 9059-9082, 1987.

Boulton, G.S., and A.S. Jones, Stability of temperate ice caps and ice sheets resting on beds of deformable sediment. *J. Glaciol., 24*, 29-43, 1979.

Catania, G.A., *A Physical Model of Pressurized Flow Over an Unconsolidated Bed: Implications for Subglacial Braided Channels*, M.S. Thesis, University of Minnesota, Minneapolis, 1998.

Clarke, G.K.C., Subglacial till: A physical framework for its properties and processes, *J. Geophys. Res., 92*, 9023-9036, 1987.

Conway, H., A. Gades, and H. Engelhardt, Ice Stream C, West Antarctica: a sticky problem, submitted for publication, 2000.

Cuffey, K., and R.B. Alley, Is erosion by deforming glacial sediments significant? (Toward till continuity), *Ann. Glaciol, 22*, 17-24, 1996.

Doake, C.S.M., R.M. Frolich, D.R. Mantripp, A.M. Smith, and D.J. Baughan, Glaciological studies on Rutford Ice Stream, Antarctica, *J. Geophys. Res., 92*, 8951-8960, 1987.

Drake, L.D., Mechanisms of clast attrition in basal till, *Geol. Soc. Am. Bull., 83*, 2159-2166, 1972.

Dreimanis, A., Tills: their genetic terminology and classification, in *Genetic Classification of Glacigenic Deposits*, edited by R.P. Goldthwait and C.L. Matsch, A.A. Balkema, Rotterdam, pp. 17-83, 1988.

Dreimanis, A., Formation, deposition, and identification of subglacial and supraglacial tills, in *Glacial Indicator Tracing*, edited by R. Kujansuu and M. Saarnisto, A.A. Balkema, Rotterdam, pp. 35-60, 1990.

Echelmeyer, K.A., W.D. Harrison, C. Larsen, and J.E. Mitchell, The role of the margins in the dynamics of an active ice stream, *J. Glaciol., 40*, 527-538, 1994.

Engelhardt, H., West Antarctic Ice Sheet: high geothermal heat flow and dynamics of ice streams, *Nature*, submitted for publication, 2000.

Engelhardt, H., and Kamb, B., Vertical temperature profile of Ice Stream B, Antarctica, *Antarctic J. U.S., XXVIII* (5), 63-66, 1993.

Engelhardt, H., and B. Kamb, Basal hydraulic system of a West Antarctic ice stream: constraints from borehole observations, *J. Glaciol., 43*, 207–230, 1997.

Engelhardt, H., and B. Kamb, Basal sliding of Ice Stream B, West Antarctica, *J. Glaciol., 44*, 223-230, 1998.

Engelhardt, H., N. Humphrey, B. Kamb, and M. Fahnestock, Physical conditions at the base of a fast moving Antarctic ice stream, *Science, 248*, 57-59, 1990.

Flint, R.F., *Glacial and Quaternary Geology*, Wiley, N.Y., 1971.

Garofalo, F., *Fundamentals of Creep and Creep-Rupture in Metals*, Macmillan, New York, 1965.

Harlan, W.B., K.N. Herod, and D.H. Krinsley, The definition and

identification of tills and tillites, *Earth Sci. Rev., 2*, 225-256, 1966.

Hindmarsh, R., Deforming beds: viscous and plastic scales of deformation, *Quat. Sci. Rev., 16*, 1039-1056, 1997.

Hill, R., *The Mathematical Theory of Plasticity*, Oxford, 1950.

Holms, C.D., Drift dispersion in west-central New York, *Geol. Soc. of Am. Bull., 63*, 993-1010, 1952.

Hooke, R.LeB., B. Hanson, N.R. Iverson, P. Janson, and U.H. Fischer, Rheology of till beneath Storglaciären, Sweden, *J. Glaciol., 43*, 172-179, 1997.

Hughes, T.J., West Antarctic ice streams, *Rev. Geophys. Space Phys., 15*, 1-46, 1977.

Hulbe, C.L., *Heat balance of West Antarctic ice streams, investigated with a numerical model of coupled ice sheet, ice stream, and ice shelf flow*, Ph.D. Thesis, University of Chicago, 1998.

Hulbe, C.L., and D.R. MacAyeal, A new numerical model of coupled inland ice sheet, ice stream, and ice shelf flow and its application to the West Antarctic Ice Sheet, *J. Geophys. Res., in press*, 1999.

Hulbe, C.L., and I.M. Whillans, Evaluation of strain rates on Ice Stream B, Antarctica, obtained using GPS phase measurements, *Ann. Glaciol., 20*, 254-262, 1994.

Iverson, N.R., R.W. Baker, and T.S. Mooyer, A ring-shear device for the study of till deformation: tests on tills with contrasting clay contents, *Quat. Sci. Rev., 16*, 1057-1066, 1997.

Iverson, N.R., T.S. Mooyer, and R.W. Baker, Ring-shear studies of till deformation, Coulomb-plastic behavior and distributed strains in glacier beds, *J. Glaciol., 44*, 634-642, 1998.

Iverson, R. M., A constitutive equation for mass movement behavior, *J. Geol., 93*, 143-160, 1985.

Jackson, M.., Dynamics of the Shear Margin of Ice Stream B, West Antarctica, Ph. D. thesis, California Institute of Technology, 1999.

Jackson, M. and B. Kamb, The marginal shear stress of Ice Stream B, West Antarctica: *J. Glaciol., 43*, 415–426, 1997.

Joughin, I., L. Gray, R. Bindschadler, S. Price, D. Morse, C. Hulbe, K. Mattar, and C. Werner, Tributaries of West Antarctic ice streams revealed by RADARSAT interferometry, *Science, 286*, 283-286, 1999.

Kamb, B., Rheological nonlinearity and flow instability in the deforming bed mechanism of ice stream motion: *J. Geophys. Res., 96*, 16,585-16,595, 1991.

Kamb, B., Glacier flow modeling, in *Flow and Creep in the Solar System: Observations, Modeling, and Theory*, edited by D.B.Stone and S.K. Runcorn, NATO ASI Series, vol. 319, pp. 417-506, Kluwer, Dordrecht, 1993.

Kamb, B., M. F. Meier, H. Engelhardt, M. A. Fahnestock, N. Humphrey, and D. Stone, Mechanical and Hydrologic Basis for the Rapid Motion of a Large Tidewater Glacier: 2. Interpretation, *J. Geophys. Res., 99*, 15,231-15,244, 1994.

Kezdi, A., *Handbook of Soil Mechanics*, Elsevier, Amsterdam, 1974.

Lambe, T.W., and R.V. Whitman, *Soil Mechanics*, J.Wiley, New York, 1969.

MacAyeal, D.R., Large-scale ice flow over a viscous basal sediment: theory and application to Ice Stream B, Antarctica, *J. Geophys. Res., 94*, 4071-4087, 1989.

MacAyeal, D.R., Irregular oscillations of the West Antarctic Ice Sheet, *Nature, 359*, 29-32, 1992.

MacAyeal, D.R., R.A. Bindschadler, and T.A. Scambos, Basal friction of Ice Stream E, West Antarctica, *J.Glaciol., 41*, 247-262, 1995.

Marone, C., C.B. Raleigh, and C.H. Scholz, Frictional behavior and constitutive modeling of simulated fault gouge, *J. Geophys. Res., 95*, 7007-7025, 1990.

Meer, J.J.M. van der, Microscopic evidence of subglacial deformation: *Quat. Sci. Rev., 12*, 553-587, 1993.

Meer, J.J.M. van der, Subglacial processes revealed by the microscope: particle and aggregate mobility in till, *Quat. Sci. Rev., 16*, 827-831, 1997.

Mercer, J.H., West Antarctic Ice Sheet and CO_2 greenhouse effect: a threat of disaster, *Nature, 271*, 321-325, 1978.

Mitchell, J.K. *Fundamentals of Soil Behavior* (2nd. ed.), Wiley, N.Y., 1993.

Nye, J.F., The flow of glaciers and ice sheets as a problem in plasticity, *Proc. Roy. Soc. London, A 207*, 554-572, 1951.

Nye, J.F., The flow of glacier in a channel of rectangular, elliptic, or parabolic cross-section, *J. Glaciol., 5*, 661-690, 1965.

Oppenheimer M., Global warming and the stability of the West Antarctic Ice Sheet, *Nature,393*, 325-332, 1998.

Raymond, C., Shear margins in glaciers and ice sheets, *J. Glaciol., 42*, 90-102, 1996.

Retzlaff, R., and C. R. Bentley, Timing of stagnation of Ice Stream C, West Antarctica, from short-pulse radar studies of buried surface crevasses, *J. Glaciol., 39*, 553-561, 1993.

Richardson, A.M., Jr., and R.V. Whitman, Effect of strain rate upon undrained shear resistance of saturated remolded Fat Clay, *Géotechnique, 13*, 310-346, 1964.

Rooney, S.T., D.D. Blankenship, R.B. Alley, and C.R. Bentley, Till beneath Ice Stream B. 2. Structure and continuity, *J. Geophys. Res., 92*, 8913-8920, 1987.

Rooney, S.T., D.D. Blankenship, R.B. Alley, and C.R. Bentley, Seismic reflection profiling of a sediment-filled graben beneath Ice Stream B, West Antarctica, in *Geological Evolution of Antarctica*, edited by M.R. Thomson et al., British Antarctic Survey, Cambridge, U.K., pp. 261-265, 1991.

Rose, K.E., Characteristics of ice flow in Marie Byrd Land, Antarctica, *J. Glaciol.,24*, 63-75, 1979.

Sheahan, T.C., C.C. Ladd, and J.T. Germaine, Rate-dependent undrained shear behavior of saturated clay, *J. Geotech. Engng., 122*, 99-108, 1996.

Scherer, R.P., Quaternary and Tertiary microfossils from Ice Stream B: evidence for a dynamic West Antarctic Ice Sheet history, *Paleogeography, Paleoclimatology, Paleoceanography, 90*, 395-412, 1991.

Scherer, R.P., A speculative stratigraphic model for the central Ross embayment, *Antarctic. J. U.S., XXIX (5)*, 9-11, 1994.

Scherer, R.P., A. Aldahan, S. Tulaczyk, G. Posnert, H. Engelhardt, and B. Kamb, Pleistocene collapse of the West Antarctic Ice Sheet, *Science, 281*, 82-85, 1998.

Scholz, C. H., Earthquakes and friction laws, *Nature, 391*, 37-42, 1998.

Shabtaie, S. and C.R. Bentley, West Antarctic ice streams draining into the Ross Ice Shelf: configuration and mass balance, *J Geophys. Res., 92*, 1311-1336, 1987.

Singh, A., and J.K. Mitchell, A general stress-strain-time function for soils, *J. Soil Mech. Found. Div. Am. Soc. Civ. Eng., 94*, 21-46, 1968.

Skempton, A.W., Residual strength of clays in landslides, folded strata, and the laboratory, *Géotechnique, 35*, 3-18, 1985.

Smith, A.M., Basal conditions on Rutford Ice Stream, West Antarctica, from seismic observations, *J. Geophys. Res., 102*, 543-552, 1997.

Smith, B., N. Lord, and C.R. Bentley, Radar studies on Ice Stream C: accumulation rates and the time of stagnation (abst.), Agenda and Abstracts, Sixth Annual WAIS Workshop, http://igloo,gsfc.nasa.gov/wais, 1999.

Terzaghi, K., R.B. Peck, and G. Mesri, *Soil Mechanics in Engineering Practice*, Wiley, New York, 1996.

Tika, T.E., P.R. Vaughn, and L.J. Lemos, Fast shearing of pre-existing shear zones in soil, *Géotechnique, 46*, 197-223, 1996.

Truffer, M., *Till Deformation Beneath Black Rapids Glacier, Alaska, and its Implications on Glacier Motion*, Ph.D. Thesis, University of Alaska, Fairbanks, 1999.

Truffer, M., W.D. Harrison, and K.A. Echelmeyer, Glacier motion dominated by processes deep in underlying till, *J. Glaciol., 45* (51), in press, 2000.

Tulaczyk, S., *Basal Mechanics and Geologic Record of Ice Streaming, West Antarctica*, Ph.D. thesis, Calif. Institute of Technology, Pasadena, Calif., 1999.

Tulaczyk, S., B. Kamb, R. Scherer, and H. Engelhardt, Sedimentary processes at the base of a West Antarctic ice stream: constraints from textural and compositional properties of subglacial debris, *J. Sed. Res., 68*, 487–496, 1998.

Tulaczyk, S., B. Kamb,. and H.F. Engelhardt, Basal mechanics of Ice Stream B, West Antarctica 1. Till mechanics, *J.Geophys. Res., 105*, 463-481, 2000a.

Tulaczyk, S., B. Kamb,. and H.F. Engelhardt, Basal mechanics of Ice Stream B, West Antarctica 2. Undrained plastic bed model, *J.Geophys. Res. 105*, 483-494, 2000b.

Tulaczyk, S., B. Kamb, and H.F. Engelhardt, Estimates of effective stress beneath Ice Stream B, West Antarctica, from till preconsolidation and till void ratio, unpublished ms., 2000.

Weertman, J., A method for setting a lower limit on the water layer thickness at the bottom of an ice sheet from the time required for upwelling of water into a borehole, *International Association of Scientific Hydrology, Publication 86*, 69-73, 1970.

Weertman, J., Glaciology's grand unsolved problem, *Nature 260*, 284-286, 1976.

Weertman, J., and G.E. Birchfield, Subglacial water flow under ice streams and West-Antarctic ice-sheet stability, *Ann. Glaciol., 3*, 316-320, 1982.

Whillans, I.M., and C.J. van der Veen, New and improved determinations of velocity of Ice Stream B and Ice Stream C, West Antarctica, *J. Glaciol., 39*, 483-490, 1993.

Whillans, I.M., M. Jackson, and Y.-H. Tseng, Velocity pattern in a transect across Ice Stream B, Antarctica, *J. Glaciol., 39*, 562-572, 1993.

Barclay Kamb, Division of Geological and Planetary Sciences, California Institute of Technology, MC 100-23, Pasadena, CA 91125